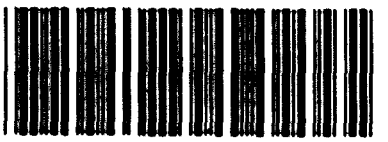

FR-8622

NRL Report 8622

Wideband HF Channel Prober: System Description

LEONARD S. WAGNER, JOSEPH A. GOLDSTEIN, AND EATHER A. CHAPMAN

Transmission Technology Branch
Information Technology Division

March 9, 1983

NAVAL RESEARCH LABORATORY
Washington, D.C.

SECURITY CLASSIFICATION OF THIS PAGE (When Data Entered)

REPORT DOCUMENTATION PAGE

READ INSTRUCTIONS BEFORE COMPLETING FORM

1 REPORT NUMBER: NRL Report 8622	2 GOVT ACCESSION NO
3 RECIPIENT'S CATALOG NUMBER	
4 TITLE (and Subtitle): WIDEBAND HF CHANNEL PROBER SYSTEM DESCRIPTION	5 TYPE OF REPORT & PERIOD COVERED: Interim report on a continuing NRL problem (6/78-6/82)
6 PERFORMING ORG. REPORT NUMBER	
7 AUTHOR(s): Leonard S. Wagner, Joseph A. Goldstein, and Esther A. Chapman	8 CONTRACT OR GRANT NUMBER(s)
9 PERFORMING ORGANIZATION NAME AND ADDRESS: Naval Research Laboratory, Washington, DC 20375	10 PROGRAM ELEMENT, PROJECT, TASK AREA & WORK UNIT NUMBERS: 61153N; RR021-05-42; 75-0141-0-2
11 CONTROLLING OFFICE NAME AND ADDRESS: Office of Naval Research, Arlington, VA 22217	12 REPORT DATE: March 9, 1983
	13 NUMBER OF PAGES: 46
14 MONITORING AGENCY NAME & ADDRESS (if different from Controlling Office)	15 SECURITY CLASS (of this report): UNCLASSIFIED
	15a DECLASSIFICATION/DOWNGRADING SCHEDULE

16 DISTRIBUTION STATEMENT (of this Report)

[redacted]

APPROVED FOR PUBLIC RELEASE
DISTRIBUTION UNLIMITED

17 DISTRIBUTION STATEMENT (of the abstract entered in Block 20, if different from Report)

18 SUPPLEMENTARY NOTES

19 KEY WORDS (Continue on reverse side if necessary and identify by block number)

HF ground wave	Channel characterization
HF sky wave	Coded ionosonde
Propagation	Pulse sounder
Wideband communication	HF channel sounder
Pulse dispersion	

20 ABSTRACT (Continue on reverse side if necessary and identify by block number)

The high-frequency, extended-line-of-sight (HF ELOS) channel, which is planned as the primary intra-task-force communication link, is a multimodal channel involving modes of widely disparate characteristics. The surface-wave mode is relatively broadband, while the sky-wave modes are substantially more limited in bandwidth because of the inherently dispersive character of the ionospheric propagation medium. Environmental factors such as sea state, seawater temperature and salinity, atmospheric-refractive-index vertical profile, and ionospheric conditions all exercise strong

(Continued)

DD FORM 1 JAN 73 1473 EDITION OF 1 NOV 65 IS OBSOLETE
S/N 0102-014-6601

SECURITY CLASSIFICATION OF THIS PAGE (When Data Entered)

20. ABSTRACT (Continued)

influences over the link characteristics. A definitive data base from which to infer the broadband signalling characteristics of the channel is not presently available.

The Wideband HF Channel Prober is a very short pulse (1-μs) HF radio sounder with the necessary sensitivity, time resolution, and processing speed to monitor and record the details of the pulse response of the channel. To exploit fully the average-power capabilities of most high-power transmitters, a coded PM sequence is transmitted rather than a single pulse. The period of the PN sequence is designed to be comparable with the expected reverberation time of the channel. Correlation processing in the receiver results in a processing of gain of the order of 34 dB. Correlations, over the entire set of delays spanning the reverberation time of the channel, permit complete recovery of the channel pulse response. Measurements are made continuously for a period of time over which the channel statistics are presumed to be stationary. Correlation, data screening, and data recording are executed in real time during the measurement procedure.

Initial experiments have been conducted over a 126-km overwater path between a high-power transmitter on San Clemente Island off the coast of southern California and a receiving site at Point Mugu on the southern California coast. Preliminary results showing the dispersive character of the F2-layer return and the channel response to an F-layer disturbance are included to illustrate the power of the instrument for studying the dynamics of the HF channel.

CONTENTS

WIDEBAND HF CHANNEL PROBER: SYSTEM DESCRIPTION

BACKGROUND

The high-frequency (HF) (2- to 30-MHz) extended-line-of-sight (ELOS) channel is a linear, time-variant, multipath channel. The primary multipath components consist of a vertically polarized surface-wave propagation mode and a variety of single- and multiple-hop E- and F-layer sky-wave reflection modes. The HF band has a number of attributes which have made it attractive for Navy intra-task-force (ITF) communications. Primary among these are that the surface-wave mode is broadband, is capable of reliable communication over task-force distances, and yet is essentially local in coverage. Another important attribute of the HF ELOS channel is that the surface wave and sky wave are independent but complementary channels, and this factor can be exploited to improve link availability. In contrast to satellite links, the HF ELOS channel does not require centralized nodes which could be vulnerable to attack. Finally, a vast amount of experience with HF equipment and operational techniques already exists in the fleet.

The HF band has certain negative attributes which, in the past, have led to a search for alternatives for fleet communications. These include requirements for large antennas, strong interaction between transmitting and receiving facilities aboard a single naval vessel, a crowded and noisy spectrum, and multipath interference. In addition, the sky-wave modes are essentially global in coverage (a negative factor in ITF communication) and depend for their existence upon the ionosphere, a highly variable and, in some geographical locations, a highly unreliable propagation medium. Despite these drawbacks, the positive factors associated with the surface-wave mode, the complementary aspects of the sky-wave modes, the potential for distributed networking, and the potential for alleviating spectrum congestion through the use of spread-spectrum techniques have all contributed to the emergence of HF as the communication band of choice for the ITF application.

The anticipated use of spread-spectrum modulation techniques highlights the importance of a large coherence bandwidth for the channel. The surface wave over a highly conducting surface is inherently broadband, and this represents one of its most attractive features. Measurements of surface-wave dispersion and associated coherence bandwidth are sparse. Measurements that are available [1] indicate a lower bound for the coherence bandwidth on the order of 0.8 MHz. This result is based on a limited set of measurements taken under a limited set of environmental conditions. An extended set of measurements at all HF frequencies and under a variety of environmental conditions and geometrical configurations is required to define completely the performance capabilities of the channel. The HF Channel Prober will provide a characterization of the channel to a bandwidth of 1 MHz.

Surface-Wave Mode

The surface-wave component is present at all times, and its attenuation depends strongly upon water temperature, salinity, sea state, and radio frequency, with higher frequencies suffering more attenuation [2]. Curves of basic transmission loss* (BTL) vs range, based on calculations by Barrick [2] for a smooth sea (conductivity = 4 S/m), and for selected frequencies in the HF band, are shown in Fig. 1. A comparison of these results with the free-space BTL at frequencies of 3, 10, and 30 MHz is shown in Fig. 2. The results are surprising in that the surface-wave attenuation remains close to the

Manuscript approved July 20, 1982.

*Basic transmission loss is defined as the ratio of transmitted to receive power when isotropic antennas are used at both sites.

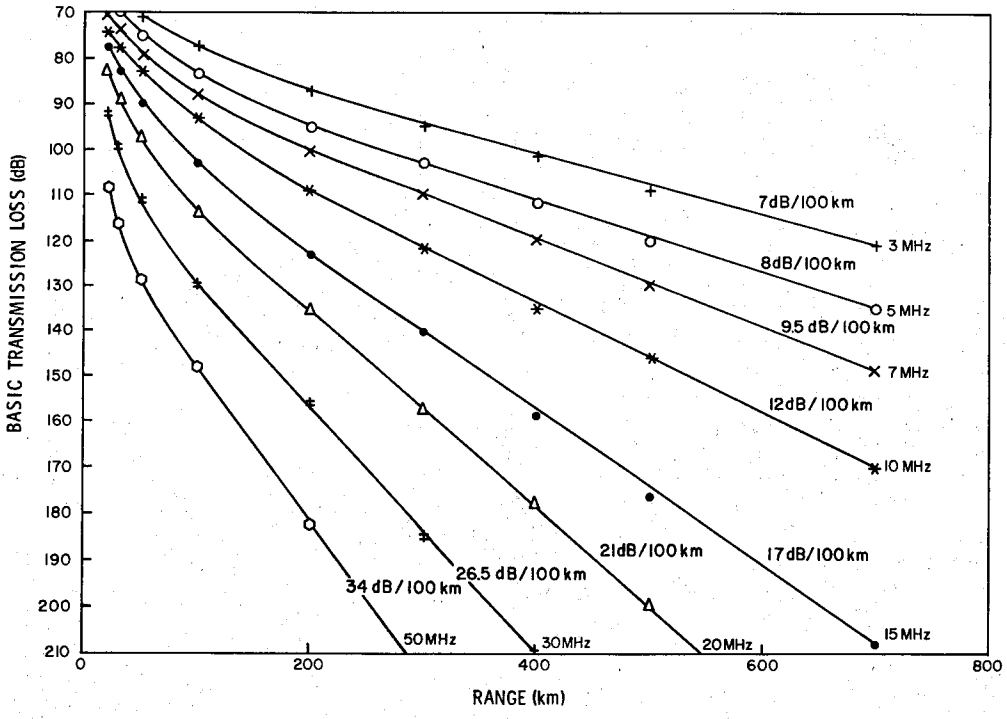

Fig. 1 — Ground-wave basic transmission loss for finitely conducting smooth sea; vertical polarization, conductivity = 4 S/m

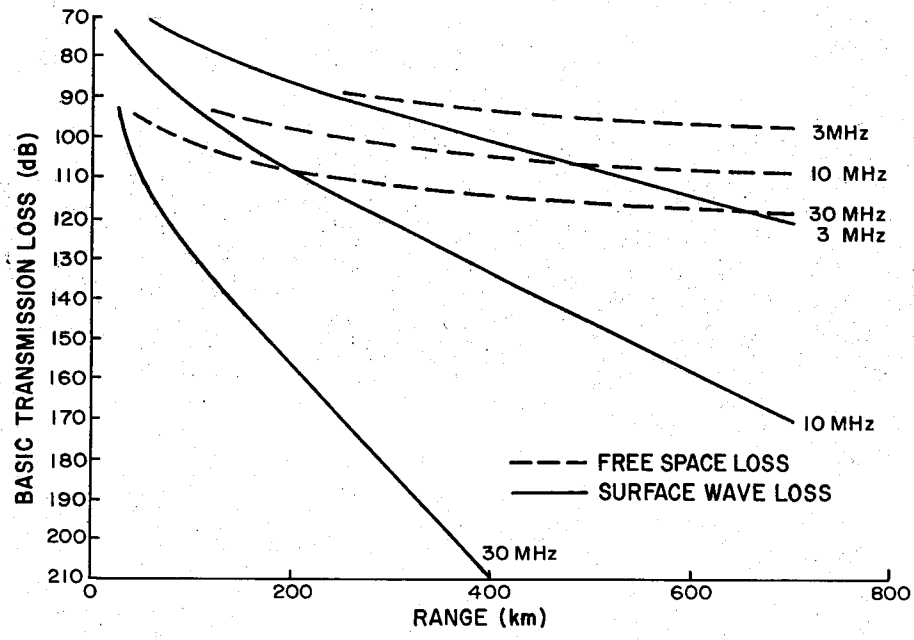

Fig. 2 — Basic transmission loss: ground-wave vs free-space loss

free-space value, especially at the lower frequencies, out to ranges of the order of several hundred kilometers

Aside from sea conductivity and factors affecting ducting, the single most important variable affecting surface-wave propagation is sea-surface roughness Waves on the sea surface serve to scatter energy out of the direct wave and into other modes, including evanescent waves. The effect of this scattering is to contribute to enhanced signal attenuation, multipath signal dispersion, and direct-path dispersion.

Scattering by surface waves occurs by the mechanism of Bragg resonant scatter. It is a well-known result that gravity waves on the sea must have a wavelength at least one half the radio wavelength in order to contribute to the real scattering of energy out of the incident wave. A prevailing wind over the ocean produces a spectrum of waves from wavelengths of the order of centimeters to a maximum wavelength determined by the wind velocity. The maximum wavelength is achieved in a fully developed sea in which the wind has been sustained over a sufficiently long distance (fetch) and for a sufficiently long time This relationship is summarized in Fig 3, which graphs maximum wavelength in meters vs wind velocity in knots Combining this result with the previously mentioned requirement that the water wavelength must exceed half the radio wavelength for real energy scatter leads to a relationship between wind velocity (or sea state) and the lowest frequency susceptible to scatter. The results, in Fig 4, show that for a wind velocity of 5 knots only frequencies above 35 MHz are scattered At a wind speed of 10 knots (sea state 2) all frequencies above 9 MHz are influenced by Bragg resonant scatter, but those below 9 MHz are not significantly scattered For a wind speed of 20 knots (sea state 4) the entire HF band is affected by scatter of energy out of the beam.

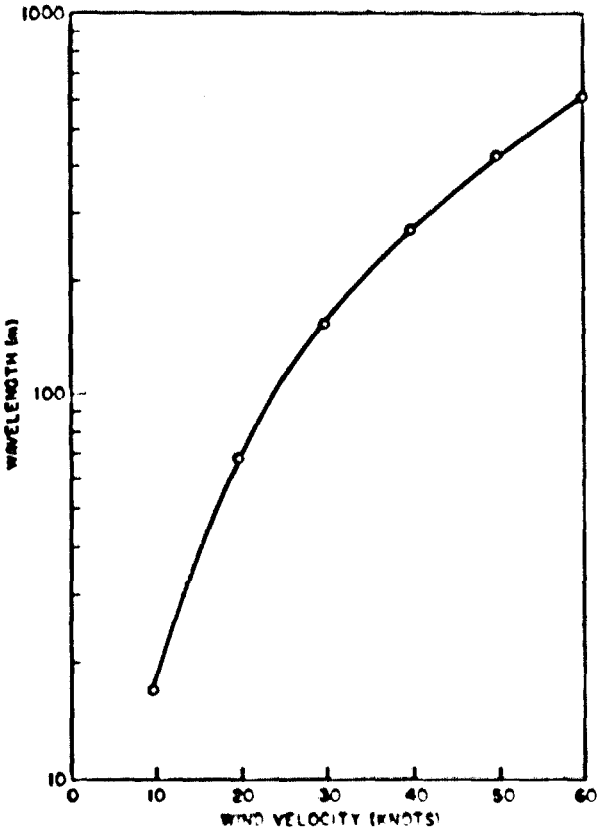

Fig 3 — Longest wavelength vs wind velocity for gravity waves on the sea surface

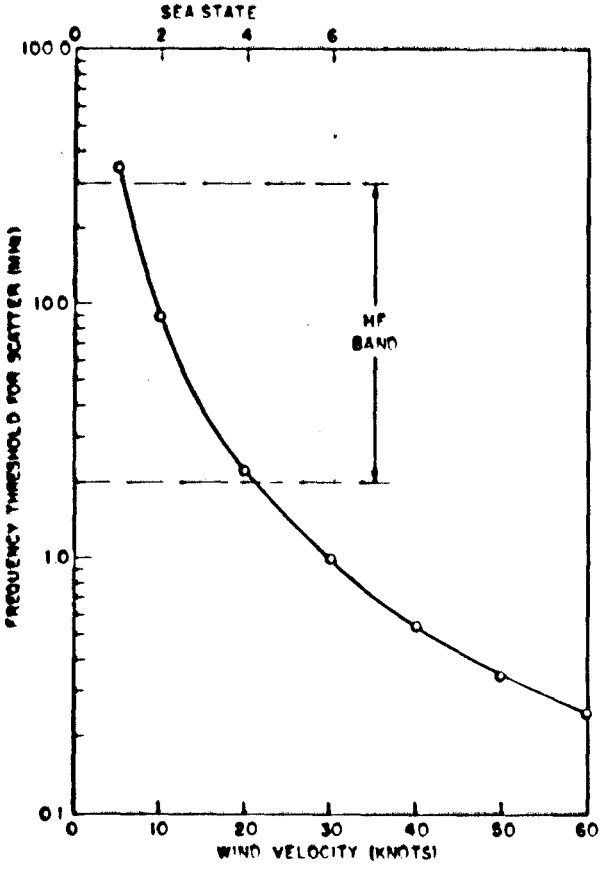

Fig 4 — Lowest frequency subject to Bragg resonant scatter vs wind velocity

The effect of sea roughness on surface wave attenuation, as calculated by Barrick [2], for frequencies of 3, 5, 10, and 20 MHz, is given in Figs. 5 to 8. Measurements by Hansen [3] over a 235-km sea path generally tend to confirm Barrick's path-loss calculation, except at frequencies above 20 MHz. It is presumed that these discrepancies are due to ducting, a not uncommon phenomenon in southern California, where the measurements were made. Some of Hansen's results are reproduced in Fig. 9. Additional results are available from the Teal Wing experiments [1], which also tend to confirm Barrick's calculations. Barrick's results (shown in Figs. 5 to 8) generally confirm the predictions of the previous paragraph regarding wind conditions required for significant surface scattering effects.

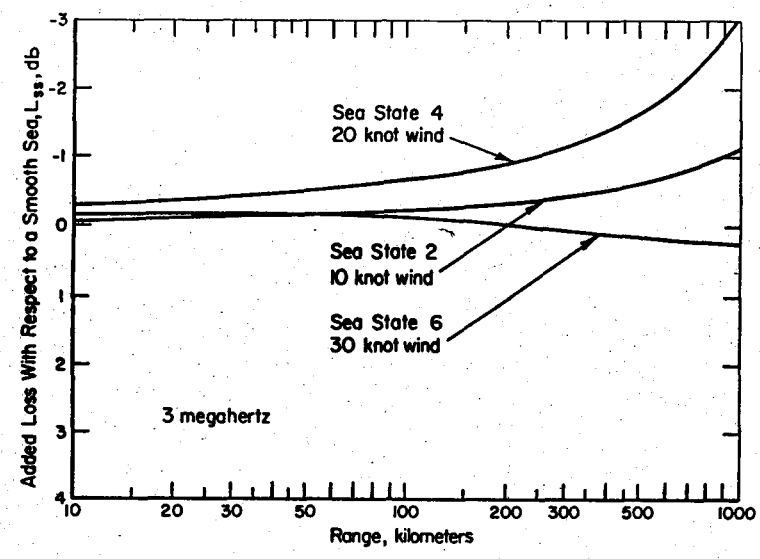

Fig. 5 — Added transmission loss due to sea state at 3 MHz (from Barrick [2], © American Geophysical Union)

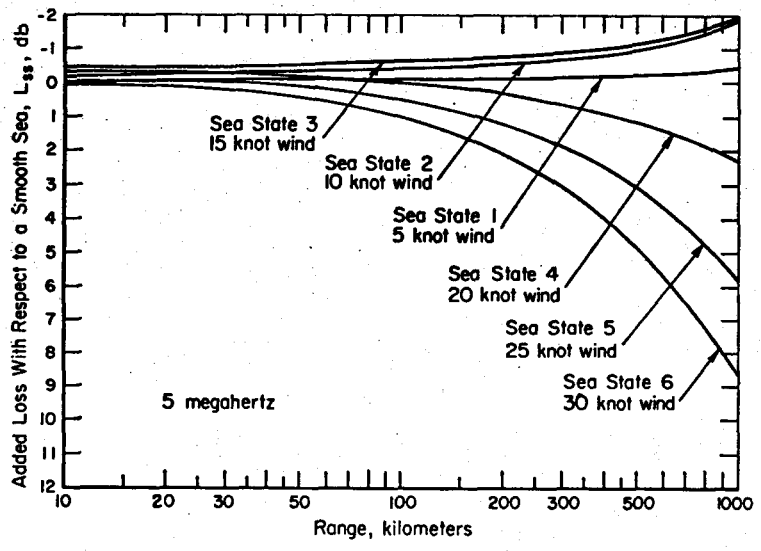

Fig. 6 — Added transmission loss due to sea state at 5 MHz (from Barrick [2], © American Geophysical Union)

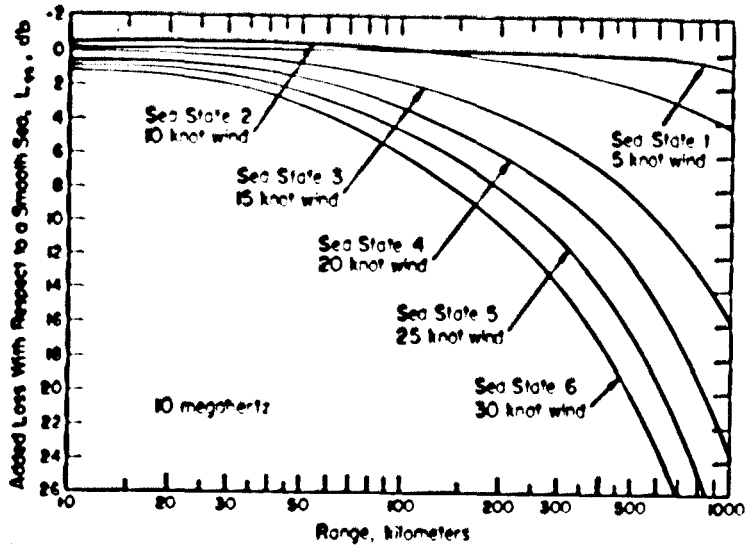

Fig. 7 — Added transmission loss due to sea state at 10 MHz (from Barrick [2], © American Geophysical Union)

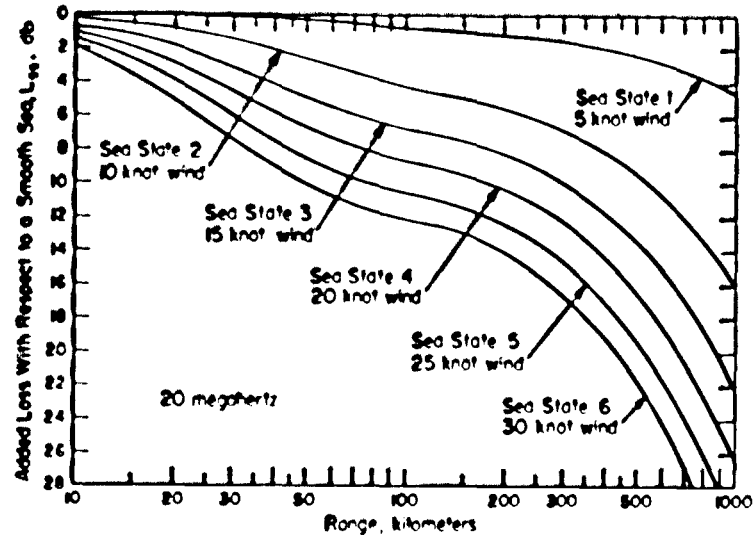

Fig. 8 — Added transmission loss due to sea state at 20 MHz (from Barrick [2], © American Geophysical Union)

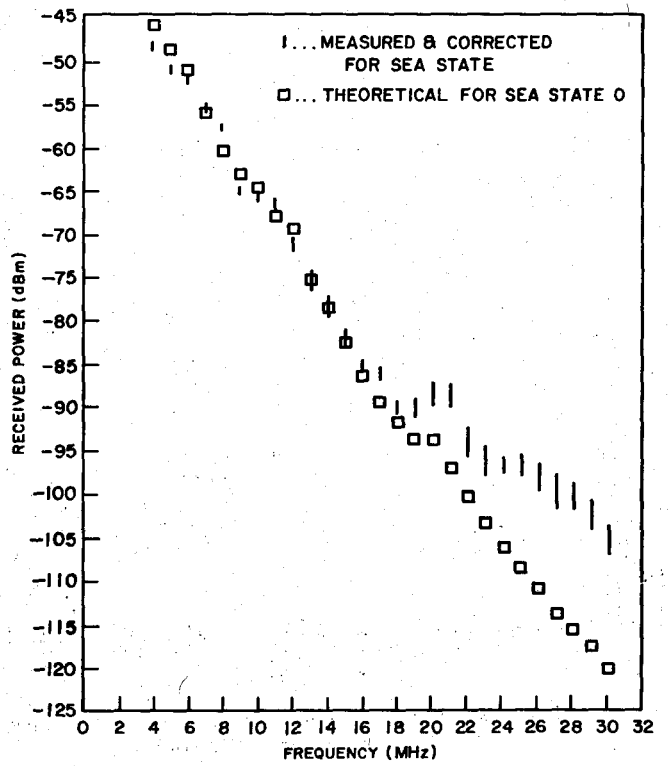

Fig. 9 — Average received-signal strength corrected for sea state (adapted from Hansen [3], © American Geophysical Union)

Sea roughness can cause signal dispersion as well as signal attenuation. Dispersion has two main sources: (1) frequency-dependent modification of the propagation characteristics of the medium and (2) development of a diffuse component resulting from energy scatter out of the transmitted wave and in the direction of the receiver. The former results in dispersion of the specular component. The latter causes dispersion by providing a multipath continuum. Conditions required for scatter are governed by the parameters summarized in Fig. 4.

Sky-Wave Modes

Skywave modes propagate by reflection (more accurately refraction) in the underside of the ionosphere, where the refractive index depends on frequency and electron density. The ionosphere may be characterized in terms of a plasma-frequency height profile. The plasma frequency is a characteristic bulk oscillation frequency of the medium and is proportional to the square root of the local electron density. For vertical incidence, it defines the highest frequency that will be reflected by the electron plasma at that height.

The lower ionosphere is composed of D, E, F1, and F2 layers. The layers impart characteristic features to the ionospheric profile, such as a ledge, an inflection point, or a localized peak value of electron density. The different layers are associated with different solar-radiation bands, different ionic constituents, and different physical processes predominating in their formation. Each layer is usually associated with an identifiable group of radio waves reflected at the altitude where the layer predominates. Such groups are characterized as E-, F1-, or F2-layer modes. Modes that experience multiple reflections along the transmission path are labeled multihop modes.

A representative ionospheric electron-density profile for summer, daytime, mid-latitude conditions is shown in Fig. 10. The profile is characterized by an ordinary E layer, at a height of 110 km, with an

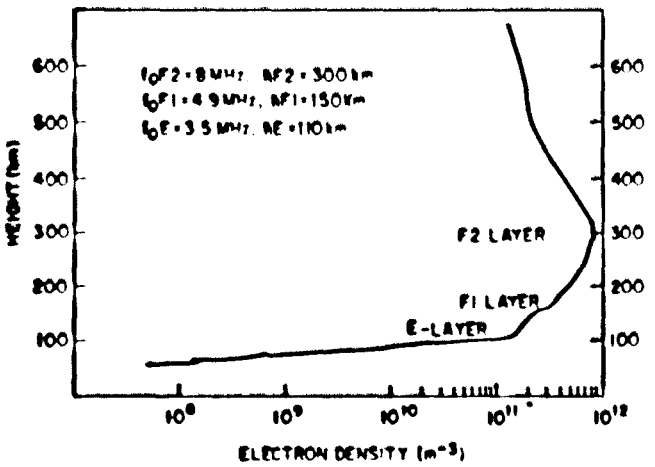

Fig. 10 — Representative electron-density profile

associated critical frequency, f_0E, (peak plasma frequency) of 3.5 MHz; an F1 layer at 150 km with a critical frequency, f_0F1, of 4.9 MHz; and an F2-layer peak at 300 km with a critical frequency, f_0F2, of 8 MHz. A simple ray-trace through this ionosphere using a radio frequency of 10 MHz, for elevation angles between 0° and 90° at 1° intervals, is shown in Fig. 11. This ray-trace serves to illustrate several important phenomena associated with sky-wave propagation. The radio frequency of 10 MHz exceeds the highest plasma frequency in the ionosphere, f_0F2, and hence, at sufficiently large elevation angles, the wave is capable of piercing the ionosphere and escaping Earth's environs. The phenomenon of "skip" is also illustrated in Fig. 11, in that no rays are returned to the surface at ranges less than 750 km. This phenomenon is related to the piercing of the ionosphere, since it is the high-elevation-angle rays which, were they not to escape, would be reflected and returned at the shorter ranges. The surface point labeled *A* in Fig. 11 is interesting, in that it shows the presence of a one-hop E-layer mode and a one-hop F2-layer mode at the same point. This illustrates the multimode nature of the HF channel, in that both modes contribute to the signal measured by a receiver at point *A*. Point *B* of Fig. 11 illustrates another HF sky-wave propagation phenomenon of interest to communicators. This is the presence of two single-hop F2-layer modes at point B, the low ray and the high ray. The high ray tends to be substantially more dispersed than the low ray, because it propagates to a greater height in the ionosphere, where the refractive index and group velocity are smaller and are more sensitive to small changes of frequency. From the point of view of the communicator, the high ray is usually of little interest, except for its deleterious effect on the reception of other modes.

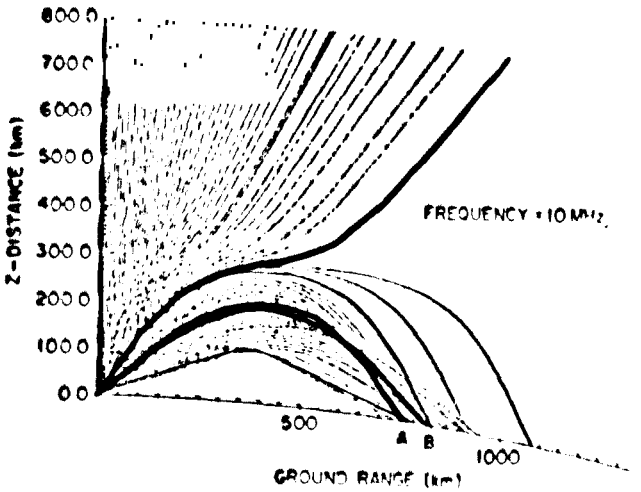

Fig. 11 — Two-dimensional ray-trace through the ionosphere of Fig. 10

Another factor, not evident from Fig. 11, is that the high and low rays merge at the skip distance. This leads to a phenomenon called skip focusing. It should be noted that, at the skip distance illustrated, 10 MHz is the maximum useable frequency (MUF). Any frequency higher than 10 MHz that is reflected would suffer less refraction and therefore would be returned at a greater range. In other words, the skip distance increases with frequency. Alternatively, for a given ionosphere, the MUF increases with range. For the short ranges involved in the intra-task-force application, the MUF is only fractionally greater than the critical frequency of the layer. Hence, frequencies substantially greater than the F2-layer critical frequency will not propagate via sky wave.

One other form of multipath propagation that can be of importance in wideband modulation systems is polarization multipath. Characteristic modes in the ionosphere consist of the elliptically polarized propagation modes, the *ordinary* and the *extraordinary*. These modes propagate with distinct group velocities and can be received as two separate signals. The delay can be of the order of several tens of microseconds, which is easily detected in high-resolution sounder systems.

Sky-wave attenuation has three main causes, free-space spreading, focusing-defocusing effects, and D-layer absorption. The first factor is self-explanatory, while the second factor is related to the lenslike focusing effects of plasma rarefactions and the defocusing effects of plasma density enhancements. Focusing-defocusing effects are related to the nonuniform electron-density profile of the ionosphere. Focusing effects tend to occur for waves that are refracted in regions of the ionosphere that have concave local height profiles, while defocusing effects occur in regions of convex profiles. The *high ray* discussed earlier, for example, typically is reflected in a region of the ionosphere where the profile is convex.

The D layer is a region of electron density at heights below 90 km where the neutral density is sufficiently high to provide strong electron-neutral interaction and, as a consequence, strong electromagnetic energy absorption. The D-layer ionization is produced mainly by hard solar x rays and, at the lower altitudes, by solar cosmic rays. D-layer absorption is a daytime phenomenon and, as with E- and F1-layer effects, shows a marked dependence on solar zenith angle.

Examples of sky-wave BTL, calculated on the basis of representative ionospheric conditions and assuming parabolic ionospheric layer shape [4], have been calculated for summer and winter nighttime conditions (Fig. 12) and for winter daytime conditions (Fig. 13). The ionospheric conditions are representative of a Zurich sunspot number of 135, and the daytime results refer to a solar zenith angle of 20°. Each layer is characterized in the figure legend by the layer height, the layer thickness and the layer critical frequency, in that order. In Fig. 12, nighttime conditions are postulated and only an F2 layer needs to be defined. The BTL for nighttime conditions shows very little dependence on range and only a mild dependence on layer height and layer shape.

Sky-wave attenuation for daytime conditions (Fig. 13) is substantially more complicated because of the more complex electron density profile as well as the presence of D-layer absorption. The BTL for winter daytime conditions requires that the ionosphere be described in terms of two parabolic layers, an E layer and an F2 layer, as well as a D layer. D-layer absorption is defined by a model representative of Zurich sunspot number 135 [4]. The BTL curves for this case show a pronounced dependence on range. This is because the longer transmission ranges correspond to lower elevation angles and, therefore, longer D-layer path lengths. Curves for 5.5 MHz (one-hop, E) and 11 MHz, (one-hop, F2) start at a range of 500 km. Shorter ranges lie within the skip distance for these frequencies.

Curves from Figs. 1, 12, and 13 are combined in Figs. 14 and 15 to compare BTL for the ground wave over a smooth sea and the sky wave for day and nighttime conditions. These curves are meant to be representative and indicate that, during the daytime, ground-wave signals predominate at all ranges of interest for frequencies lower than 6 MHz. At night, a range of 300 km represents a rough dividing line for regions of dominance of sky wave and ground wave.

LAYER ID	PROBING FREQUENCY (MHz)	LAYER HEIGHT (km)	LAYER THICKNESS (km)	CRITICAL FREQUENCY (MHz)
---- 1-HOP F2 LAYER, WINTER NIGHT	8.5	300	80	4.0
—— 1-HOP F2 LAYER, SUMMER NIGHT	4.25	350	65	8.25

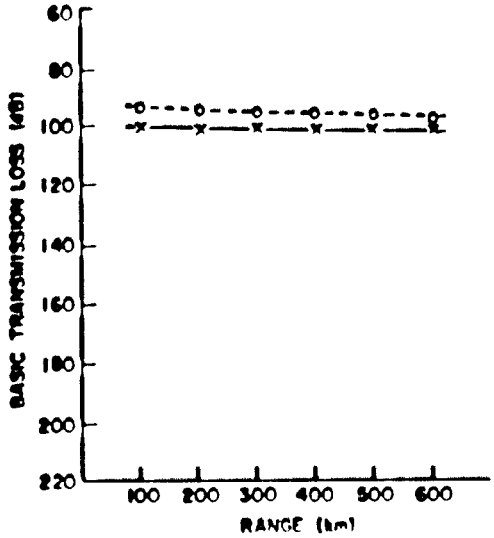

Fig. 12 — Sky-wave basic transmission loss, representative nighttime conditions

WINTER DAYTIME PROFILE

LAYER ID	LAYER HEIGHT km	LAYER THICKNESS km	CRITICAL FREQUENCY MHz
E-LAYER	110	10	2.8
F2-LAYER	250	55	9.9

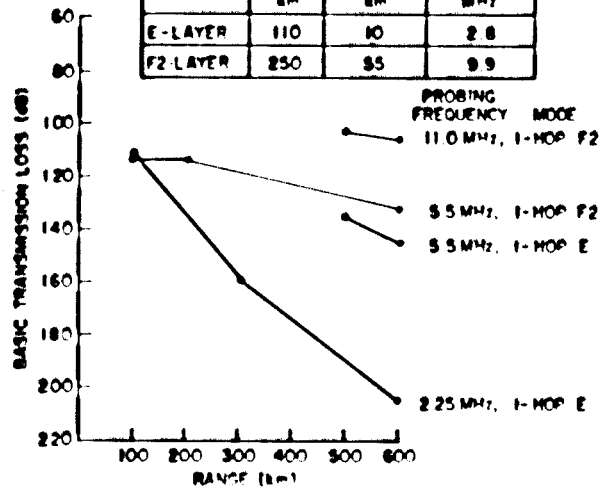

Fig. 13 — Sky-wave basic transmission loss, representative winter daytime conditions

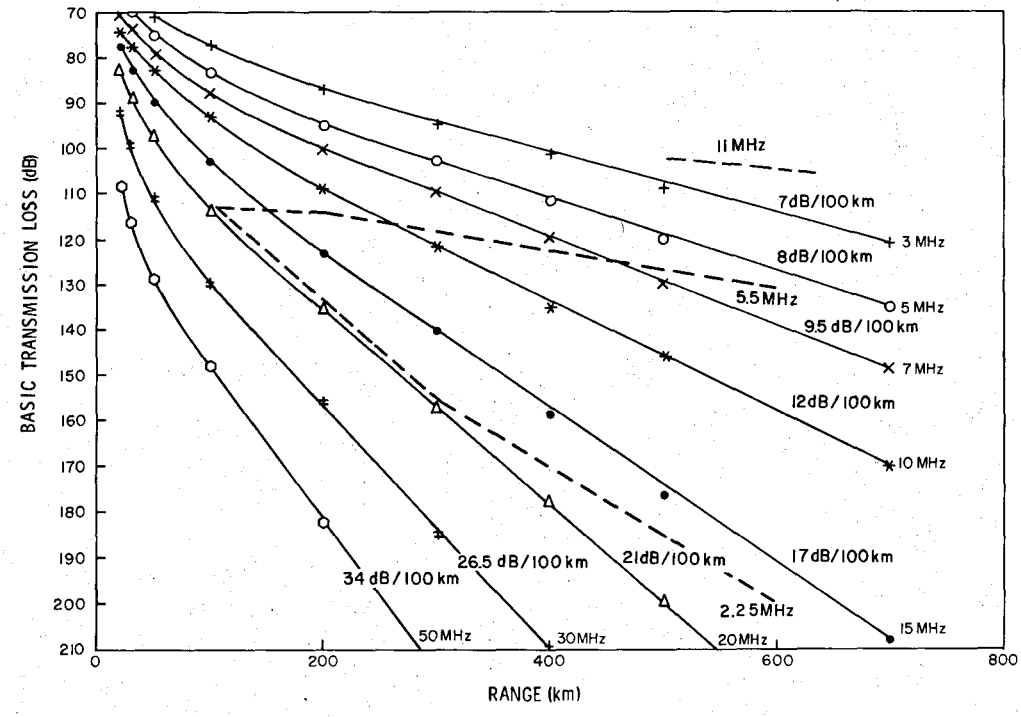

Fig. 14 — Basic transmission loss for ground wave over a smooth sea vs sky wave for winter daytime conditions

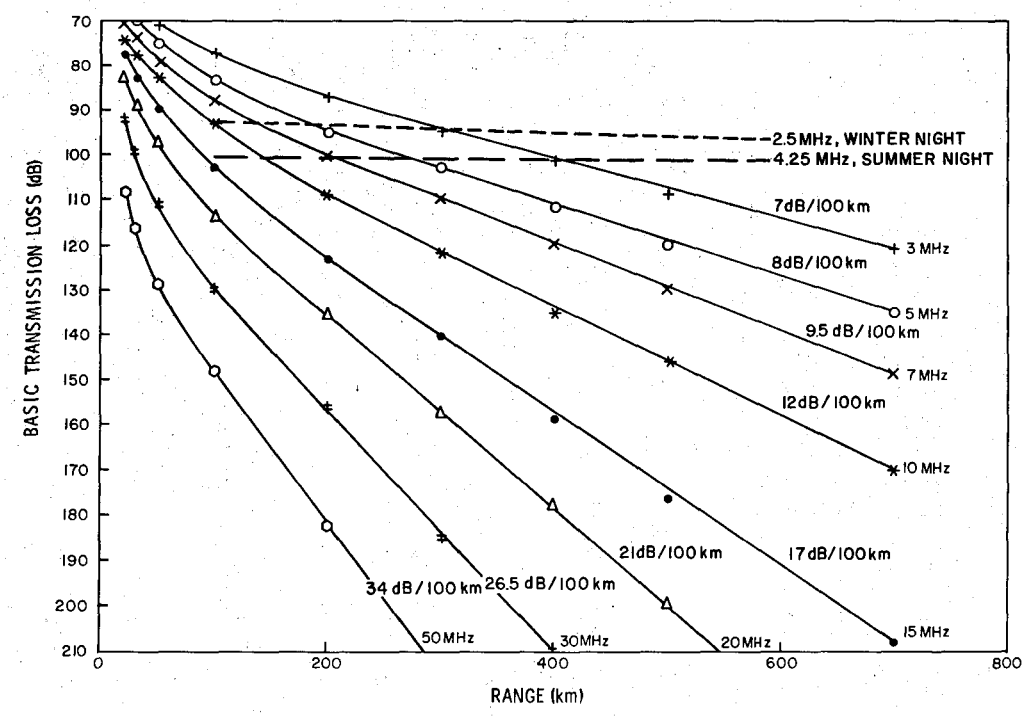

Fig. 15 — Comparison of basic transmission loss for ground wave over a smooth sea with sky wave for nighttime conditions

CHANNEL-PROBER INSTRUMENT

Approach

The Wideband HF Channel Prober program is designed to provide measurements for a detailed description of the wideband (1-MHz), HF (2- to 30-MHz) intra-task-force communication channel. Channel characteristics of interest include:

- mode structure,
- delay power spectrum of individual modes,
- signal doppler shift and doppler spread, and
- signal statistics

A thorough description of the channel requires measurements over a wide variety of atmospheric and sea-state conditions as well as over a variety of geometries and antenna configurations.

The approach has been to construct a broadband radio sounder capable of recording the channel response to a short pulse [5]. Measurements are made continuously for a period of time over which the channel statistics are presumed stationary. Data selection and recording are executed in real time during the measurement period

To exploit fully the average power capabilities of most transmitters while still probing the medium with a narrow effective pulse, a coded, pseudo-noise (PN), binary sequence is used as a modulation signal. The period of the PN sequence is made comparable with the reverberation time of the channel which, in this case, has been estimated at 8 ms. The pulse (chip) duration has been chosen to be consistent with the bandwidth requirements of the probing signal, and the pulse duty factor has been chosen to be within the duty factor constraints of certain high-power radar transmitters known to be available for use. Correlation processing in the receiver over the entire set of time delays spanning the channel reverberation time leads to the complete recovery of the channel pulse response. A functional block diagram of the Wideband HF Channel Prober is shown in Fig. 16.

The Wideband HF Channel Prober is designed to operate in one of two different bandwidth modes. The narrowband Sounder mode involves a system bandwidth of 125 kHz. The data rate in this mode is within the real-time capabilities of the system, so that all correlator output samples are processed and stored. The Sounder mode provides data for characterizing the ionospheric medium in a conventional manner and for preparing the system to cope with the flood of data generated in the wideband, 1-MHz mode. In addition, Sounder-mode data are useful in those applications for which 125-kHz-bandwidth data suffice. Correlation processing in the Sounder mode provides a nominal 24 dB of processing gain.

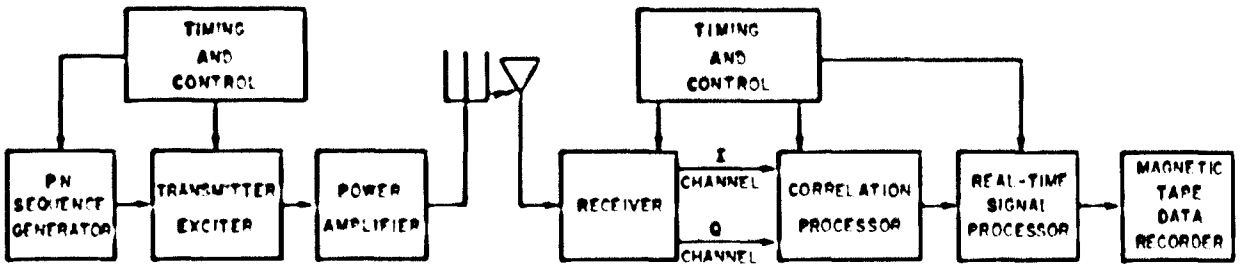

Fig. 16 — Wideband HF Channel Prober functional block diagram

In the Prober mode, channel characteristics are examined with a 1-MHz resolution bandwidth. Data are generated at eight times the rate of the Sounder mode. To cope with the increased data rate from the correlator, the real-time processor must define "time windows" during which signal information is expected. The placement of these windows is based on data acquired during earlier Sounder-mode data sampling. Data generated outside of these time windows are ignored by the real-time processor. Correlation processing in the Prober mode provides a nominal processing gain of 33 dB.

The slowest element in the data-processing chain, and therefore the one which limits data throughput, is the magnetic tape recorder. Magnetic tape was chosen as the medium of data storage because of its large capacity, ease of handling and storage, and economy. The magnetic-tape recorder is a nine-track machine which operates at a speed of 45 in./s (IPS) (114.3 cm/s) and at a density of 800 bits/in. (bpi) (315 bits/cm). This results in a maximum write rate of 36,000 bytes/s. In tests, the Wideband HF Channel Prober magnetic-tape unit has been successfully operated at an average write rate of 31,000 bytes/s.

Signal Characteristics

The waveform of the PN sequence modulation signal is shown in Fig. 17. The waveform consists of a pulsed PN sequence repeating approximately every 8 ms (the channel reverberation time). The pulse width (chip width) defines the signal bandwidth. Detailed specifications of the signal waveform for both the Sounder mode and the Prober mode are given in the table included in Fig. 17. The specifications for the Prober mode lead to a PN sequence consisting of 2047 chips derived from an 11-stage maximal-length PN sequence. For the Sounder mode, the corresponding number of chips is 255, and the sequence is derived from an 8-stage maximal length PN sequence. In Fig. 17, the sequence repetition period (T_s) is the number of chips (N) times the pulse repetition period (T). The use of a 25% duty factor serves a dual purpose: (1) it makes the signal compatible with available high-power transmitters and (2) it reduces the number of chips in the PN sequence for a given bandwidth and repetition period. The latter consideration is of great importance in terms of the required size and speed of the correlation processor at the receiver.

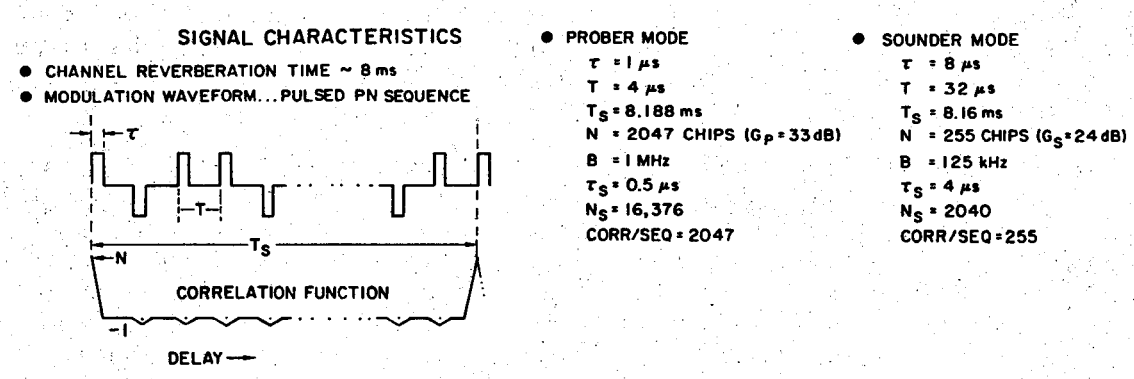

Fig. 17 — Pseudo-noise modulation characteristics

The required speed for the digital logic in the correlation processor is set by the requirements of Prober-mode real-time operation. In this mode, a sample of the pulse response must be evaluated every 0.5 μs of delay over the 8.188-ms repetition interval. This corresponds to a total of 16376 samples and therefore to a total of 16376 separate correlations. Each correlation requires essentially 2047 additions for a total of 32 × 106 digital operations per pulse response. Since the receiver splits the received signal into the in-phase (I) and the quadrature (Q) components, the number of digital operations per response is doubled. Completion of 64 × 106 digital "adds" in an 8-ms period requires a digital-logic cycle time of the order of 0.1 ns, which was deemed unachievable and impractical for the channel-prober experiment. As a "fallback" position, the correlator designer (CNR Inc.) decided to process one eighth of the correlation samples (one frame of data) during a single 8-ms reverberation inter-

val and to execute half of the sums in a preprocessor. This approach reduced the logic speed requirements to a value of 2 ns, which was deemed practical with currently available digital logic. It did, however, necessitate eight repetitions of the signal waveform for a complete definition of the pulse response. During each frame, 2047 equally spaced 0.5-μs samples are evaluated. In subsequent frames the remaining interleaved samples are evaluated as in a sampling scope.

The correlator that was finally produced used a logic clock rate of 8 MHz with an associated cycle time of 125 ns. The logic time was reduced to 2 ns through the use of parallel logic, resulting in a system consisting of 64 parallel correlators, 32 operating on the I channel and 32 operating on the Q channel. The significance of the use of a 25% duty factor together with a 1-MHz bandwidth is readily perceived at this point, since a 100% duty factor would have resulted in a PN sequence four times the size of that used and an overall processing-speed requirement four times that proposed. This would have required either digital logic capable of a 32-MHz rate or else 8-MHz logic with 256 parallel correlators split evenly between the I and Q channels. Neither of these alternatives was considered practical.

Experiment Format

The basic format for the channel-prober experiment, as presently conceived, is to start with a Sounder run and then to alternate Prober and Sounder runs. The Sounder run is used to define the state of the ionosphere. It is also a necessary prerequisite to the Prober run to determine the time windows. The Sounder run is relatively short and will usually consist of a single comprehensive sweep, in 100-kHz steps, through the frequency range of interest.

Because of the variable frequency format, radio sounders require a high degree of coordination between operations at the transmitter and receiver sites. The coordination can be accomplished either by a prescribed and relatively invariant time and frequency format or by a communication link between the two sites for defining the experiment format. Conventional sounders use the former technique, while the channel prober, which is designed for more versatile operation, uses the latter technique.

The Prober section of the experiment may be operated in a frequency-scan format, in a fixed-frequency format, or in a combination of both formats. Since the HF band is heavily used, there are some portions of the spectrum that must be avoided. In the scan format, the frequency is stepped sequentially in 1-MHz steps, with care taken to skip over proscribed bands. The fixed-frequency format is used when one desires to maintain phase coherence over longer time intervals as, for example, when one is making doppler measurements. As suggested above, a hybrid mode, in which one transmits for several correlation cycles on a given frequency and then switches to the next frequency, may provide acceptable doppler resolution while still providing a frequency-scan capability.

The Prober mode is usually maintained over a time interval comparable to the time for statistical stationarity of the channel characteristics. This time is estimated, a priori, at approximately 15 min. The duration is sufficient to permit 60 complete scans through the entire HF band when a maximum integration of eight sequences is used. The Prober mode is followed immediately by a Sounder-mode run, and comparison with the previous Sounder-mode run is used to determine if channel conditions have changed significantly during the measurement interval.

Transmitter

The transmitter block diagram is shown in Fig. 18. Equipment supplied as part of the Wideband HF Channel Prober includes all blocks in Fig. 18 except for the power amplifier and antenna, which are supplied by the host facility. The channel-prober system equipment occupies a single full-size rack plus a hard-copy terminal for the control module, as shown in Fig. 19. The channel-prober transmitting package can be used with a variety of wideband HF transmitters and was designed with transportability in mind.

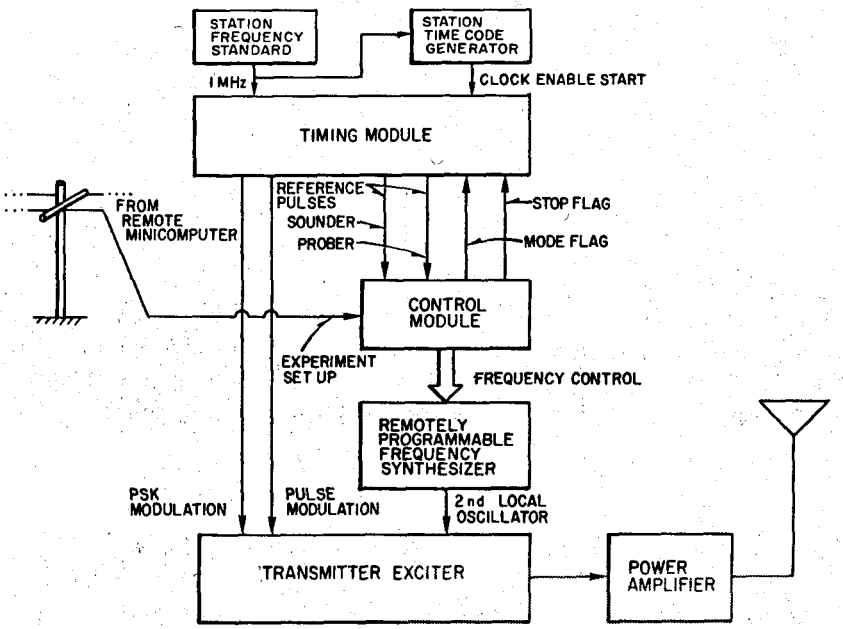

Fig. 18 — Transmitter block diagram

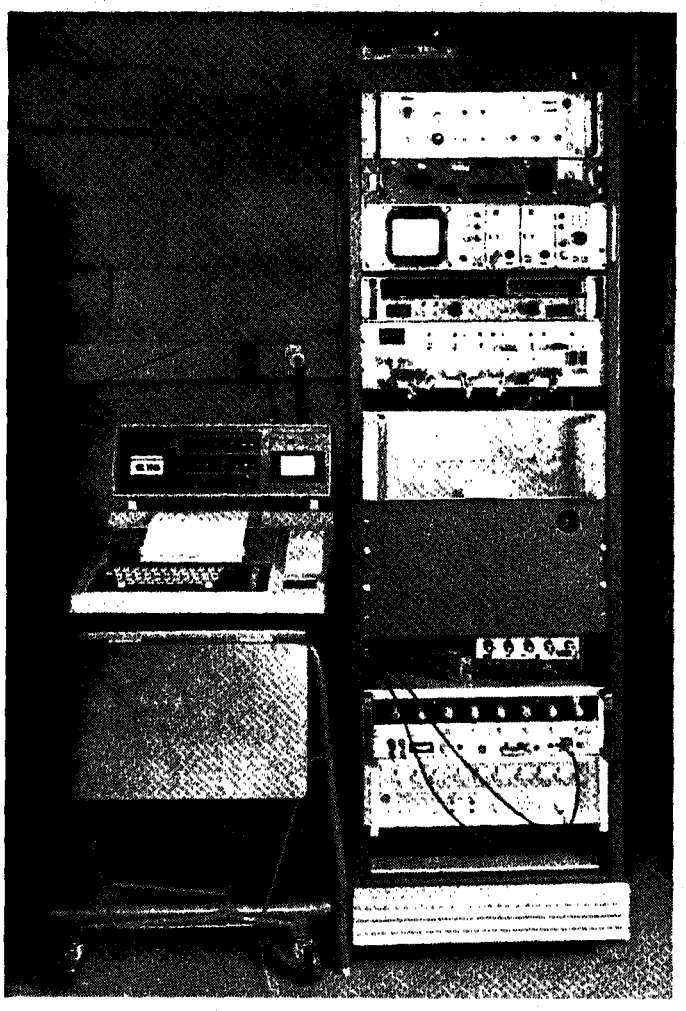

Fig. 19 — Wideband HF Channel Prober transmitter equipment

The transmitter site is equipped with a highly accurate frequency standard, which is the basis for all timing and frequency reference signals at the site. Prior to a measurement campaign, the frequency standards at the transmitter and receiver sites are aligned. Standards of sufficient accuracy have been chosen such that a single calibration suffices for roughly a 4-week period. Criteria for judging the accuracy of the frequency standards are that the doppler shift be less than the instrument's doppler resolution capability and that the time drift be sufficiently small that it is less than a pulse width during the time of a correlation cycle. The former condition is by far the more stringent and calls for a long term frequency accuracy of 4×10^{-10} per month. The station standards used are based on rubidium vapor resonance cells and have a nominal long-term accuracy of 1×10^{-11} per month.

Experiment start at the two sites is based on a prescribed start time. Digital time-code generators at the two sites are set to WWV time transmissions and relative accuracy is within ± 1 ms. This is an acceptable tolerance, since it is short compared with the basic PN sequence period and is comparable to transmission delays between transmitter and receiver.

The major system components at the transmitter site are the timing module, the control module, the transmitter exciter, and the host power amplifier and antenna system.

Timing Module

The timing module generates timing and modulation signals used in system operation. It contains a time comparator circuit for generating a "clock start" logic signal at the prescribed experiment start time. It also generates the PN sequences used in the binary phase shift key (BPSK) modulation of the transmitter-exciter carrier and the pulse-modulation signal for developing the 25% duty factor. These signals are generated simultaneously and continuously for both the Sounder and Prober modes of operation, with the appropriate sequence logically gated to the exciter by control signals developed in the control module. At a fixed reference point in each PN sequence, a reference pulse is supplied to the control module. These reference signals are treated as interrupts by the control module and thereby enable it to count the number of executed sequences and to control the experiment operation.

Design details of the timing module are covered in a separate report devoted to the timing and control modules for the Wideband HF Channel Prober [6].

Control Module

The control module controls the experiment format at both the transmitter and receiver sites in a coordinated and synchronized manner. It is implemented by a microprocessor (Motorola model 6802 MPU) which stores the frequency format and all other experiment parameters in RAM memory. The frequency format and the experiment constants are communicated from the remote receiver site where experiment control is resident. The communications link is via telephone circuits.

Based on the number of reference pulses received from the timing module, the control module determines when to step in frequency, when to switch modes, and when to terminate the run. Depending on frequency and mode, the control module supplies frequency information, as BCD voltage levels, for remote control of a synthesizer used as the local oscillator in the exciter down-converter. In addition, the mode flag generated by the microprocessor control module is used to gate the appropriate modulation signals to the exciter and to switch filters according to mode. Reference pulses associated with the Sounder and Prober PN sequences are simultaneously received and one or the other is enabled as an interrupt according to the prevailing mode, as determined by a flag in the microprocessor.

Software and hardware details of the control module are described in a separate report covering design details of the timing and control modules [6].

Transmitter Exciter

The transmitter exciter, Fig. 20, generates a fixed-frequency (39.5-MHz) carrier, which is pulse and phase (BPSK) modulated by the pulse train and PN sequence supplied by the timing module. The 39.5-MHz carrier is generated by a General Radio (GR) model 1164-A phase-locked-loop synthesizer, which is locked to the 5-MHz station standard. The spurious discrete components of the output are 60 dB below the fundamental. The harmonics are at least 30 dB below the fundamental at maximum output of 19 dBm (2 V rms into 50 Ω) and smaller at lesser outputs. The modulated 39.5-MHz carrier is passed through a bandpass filter of bandwidth 1 MHz or 125 kHz, depending on mode. The 1-MHz filter is a six-pole, modified Butterworth tubular bandpass filter (BPF). The 125-kHz-bandwidth filter is a four-pole, modified Butterworth tubular bandpass filter. The filters were chosen to provide a suitable compromise between their cutoff characteristics in the frequency domain and the amplitude of their sidelobes in the time domain. Amplitude and phase characteristics of these filters are shown in Figs. 21 and 22. The different paths for the Sounder- and Prober-mode signals are suitably padded for transmitter output equalization to within 1 dB. The filter output is passed through a down-converter whose local oscillator frequency is determined by the control module in such a way that the mixer output is at the desired frequency. The local oscillator (2nd LO) is a Programed Test Sources (PTS) model 160 direct-frequency synthesizer, with BCD inputs for remote control of frequency and with a 5-MHz station standard reference frequency. The PTS synthesizer has a nominal switching time of 20 μs, discrete spurious components that are 75 dB below the fundamental, harmonics that are at least 35 dB below the fundamental, a noise floor of -135 dB/Hz, and phase noise of -63 dBc in the band 0.5 Hz to 15 kHz. The amplifiers in Fig. 20 are Anzac models AM-109 and AM-127 and have 10-dB gain.

The output of the down-converter is amplified and passed through a low-pass filter for attenuation of out-of-band components. The filter is a 15-pole Zobel type. The filter transfer characteristic is shown in Fig. 23.

The exciter output pulse shape for Sounder and Prober modes is shown in Fig. 24. The Sounder-mode pulse was recorded for an exciter output frequency of 25 MHz and exhibits no discernible time sidelobes. The Prober-mode pulse was recorded for an output frequency of 10 MHz and exhibits a time sidelobe of -19.5 dB relative to the main pulse.

Host Power Amplifier and Antenna System

It is anticipated that the Wideband HF Channel Prober will be capable of operating in conjunction with a number of different power amplifier/antenna systems. The system used initially is the "Sea-Echo" radar transmitter on San Clemente Island, Fig. 25. The antenna array consists of 25 vertical half-rhombic elements with three selectable antenna lengths. The array azimuthal beamwidth is 2° at 16 MHz and can be extrapolated to other frequencies according to inverse wavelength. Figure 26 illustrates the gain variation vs frequency for the three rhombic antenna lengths at an elevation angle of 2°. Figure 27 shows antenna elevation patterns at 6.0 MHz for the three antennas and for two different element-phasing arrangements. Figure 27a illustrates the elevation pattern obtained for equal phase weighting of all the elements, resulting in a broadside radiation pattern. The elevation pattern obtained in this case is identical to that of a single element. Figure 27b corresponds to the elevation pattern obtained when the array is phased for a main beam in the direction of Point Mugu. The patterns of Fig. 27b are representative of the types of elevation patterns to be expected. A detailed description of the antenna design and configuration is given in Ref. 7.

Each element of the array is driven by a separate power amplifier capable of delivering an average output of 500 W. The amplifiers are designed for a maximum duty factor of 33%. The system is capable of an average output power of 12.5 kW. A complete description of the power amplifier is given in Ref. 8.

HF CHANNEL PROBER EXCITER

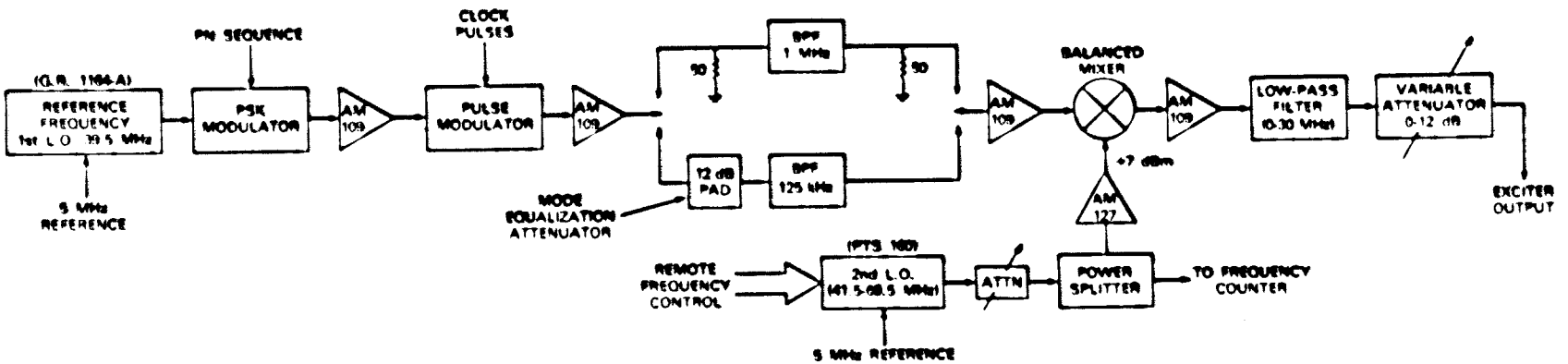

Fig. 20 — Exciter block diagram

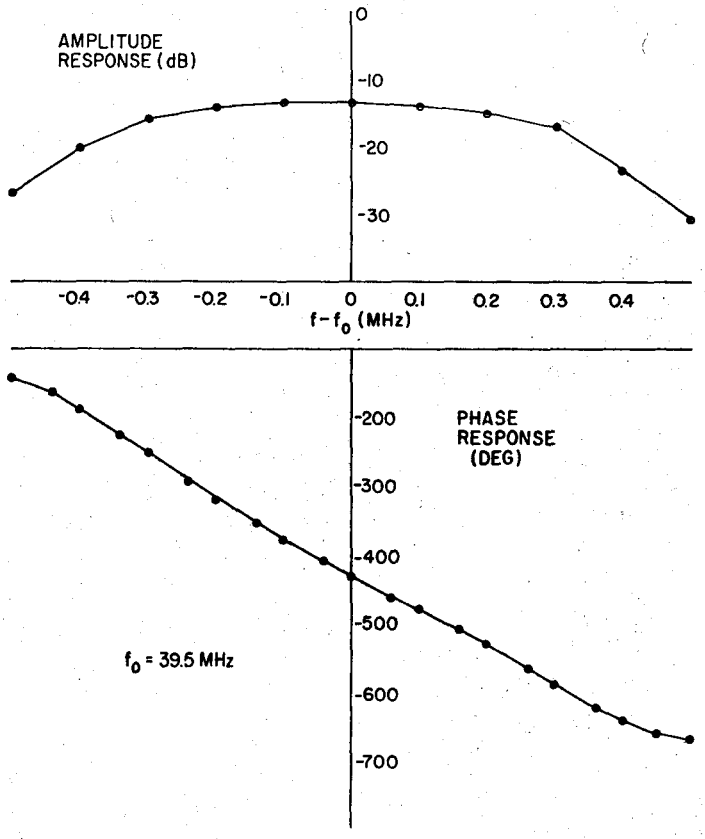

Fig. 21 — Exciter IF-filter characteristic, Sounder mode

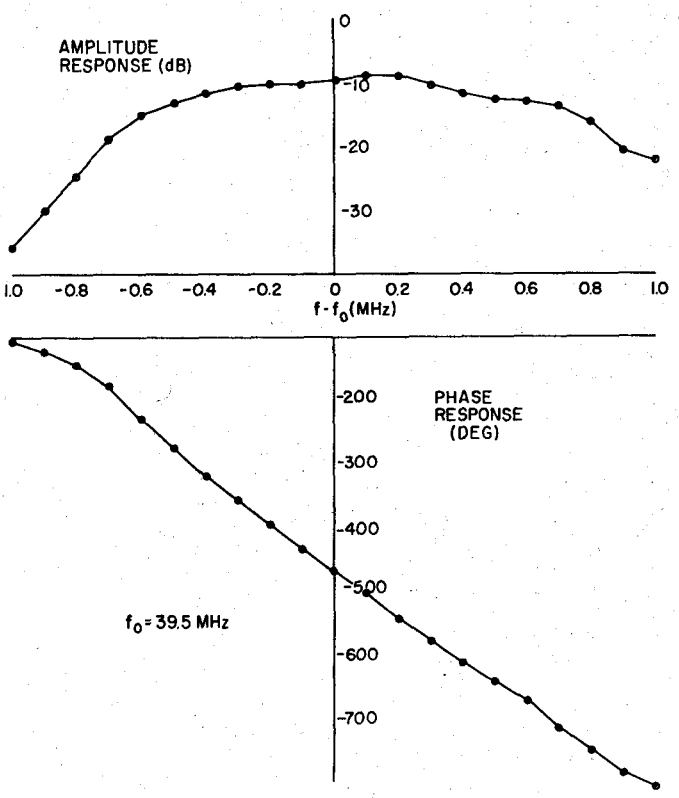

Fig. 22 Exciter IF-filter characteristic, Prober mode

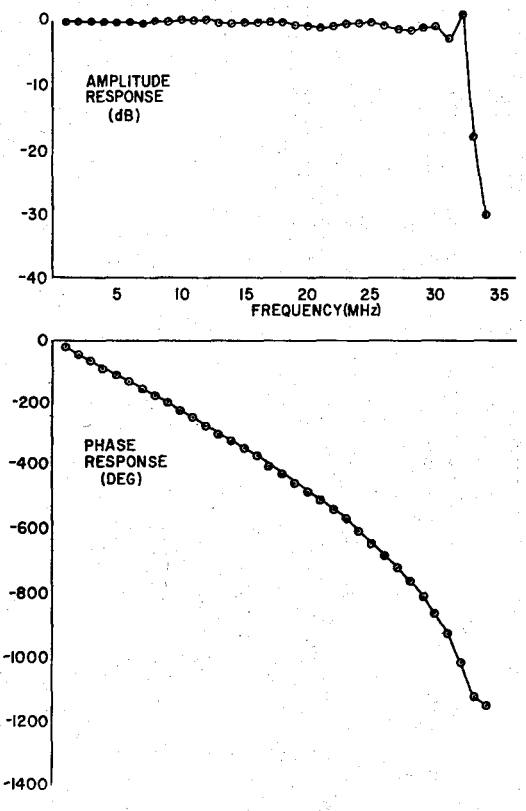

Fig. 23 Exciter low-pass-filter characteristic

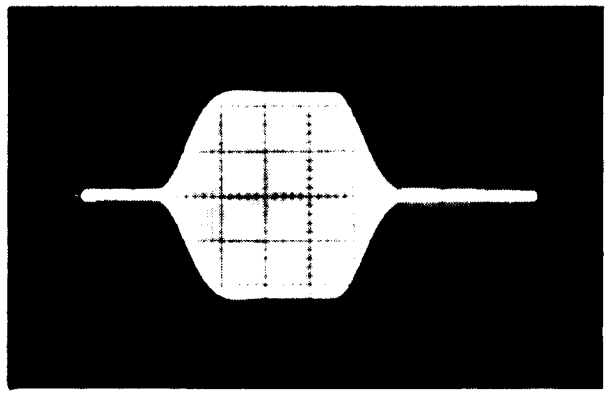

(a)

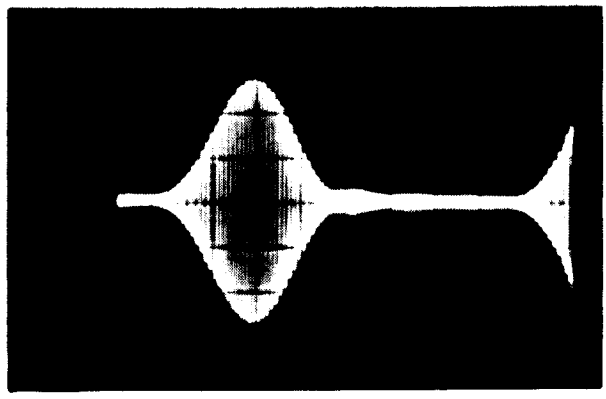

(b)

Fig. 24 — Exciter pulse shape: (a) Sounder mode, 2 μs/div horizontal, 0.05 V/div vertical, (b) Prober mode, 0.5 μs/div horizontal, 0.05 V/div vertical

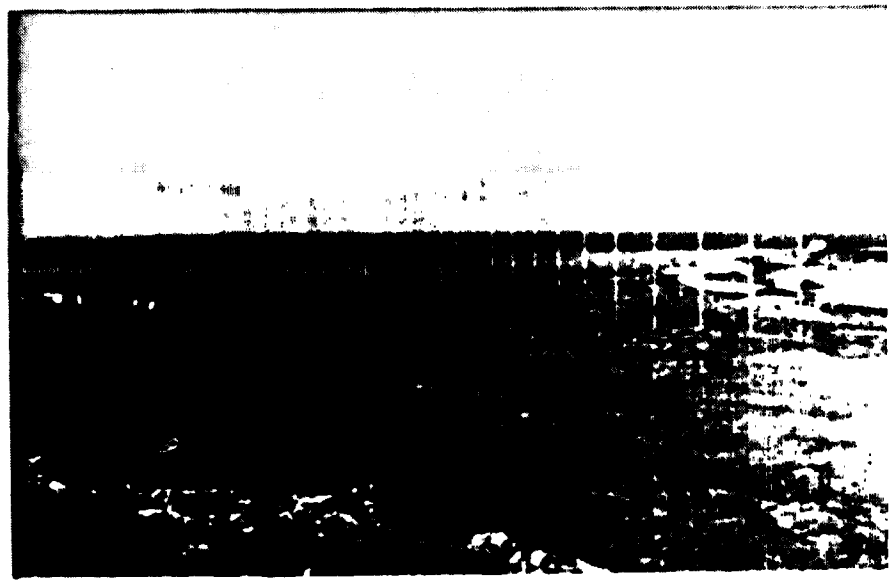

Fig. 25 — Transmitting antenna array

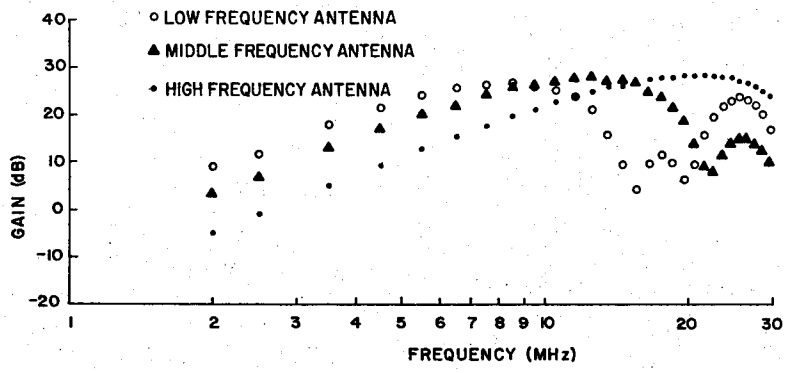

Fig. 26 — Transmitting-antenna gain vs frequency at elevation angle of 2° (one-way gain)

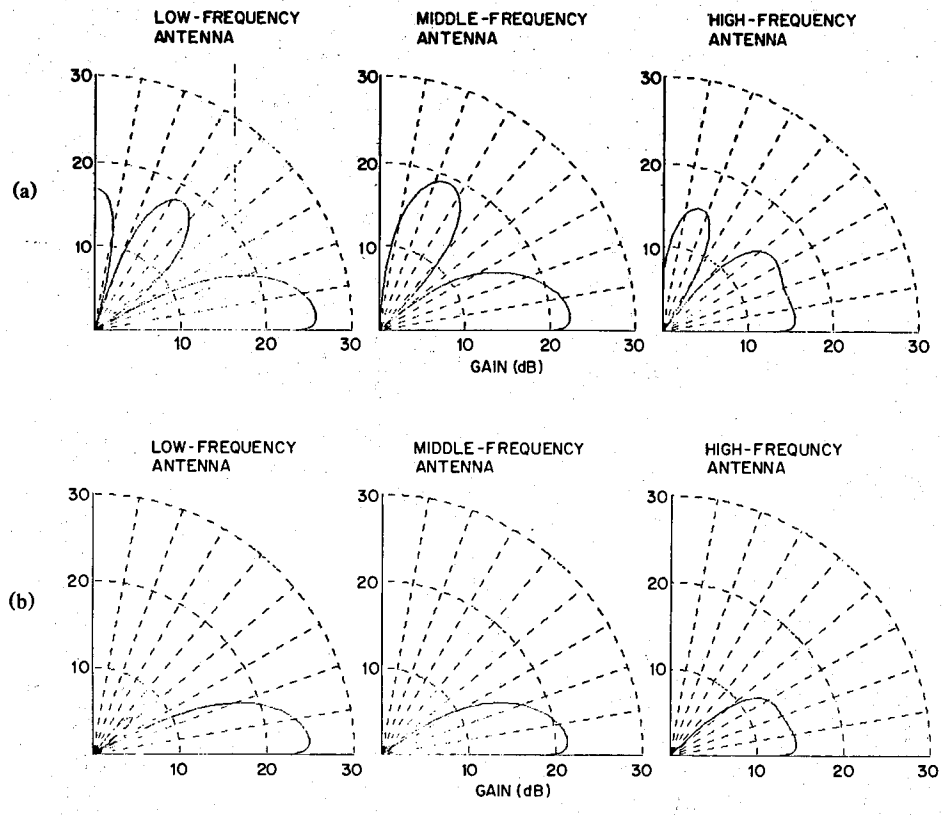

Fig. 27 — Transmitting-antenna elevation pattern at 6 MHz: (a) Elevation pattern for broadside main lobe; (b) Elevation pattern for main lobe pointing in the direction of Point Mugu

Receiver

The receiving-system block diagram is shown in Fig. 28. The station frequency standard, the timing module, and the control module operate in precisely the same manner and perform the same functions as at the transmitting site. At the receiving site the control module has the added responsibility of providing the real-time processor (Digital Equipment Corp. [DEC] model PDP-11/34 minicomputer) with detailed information regarding operating mode, frequency pointer, AGC-sample timing, and correlation-start synchronization. Modules unique to the receiver site are the antenna-preamplifier, the HF receiver, the correlation processor and the real-time processor.

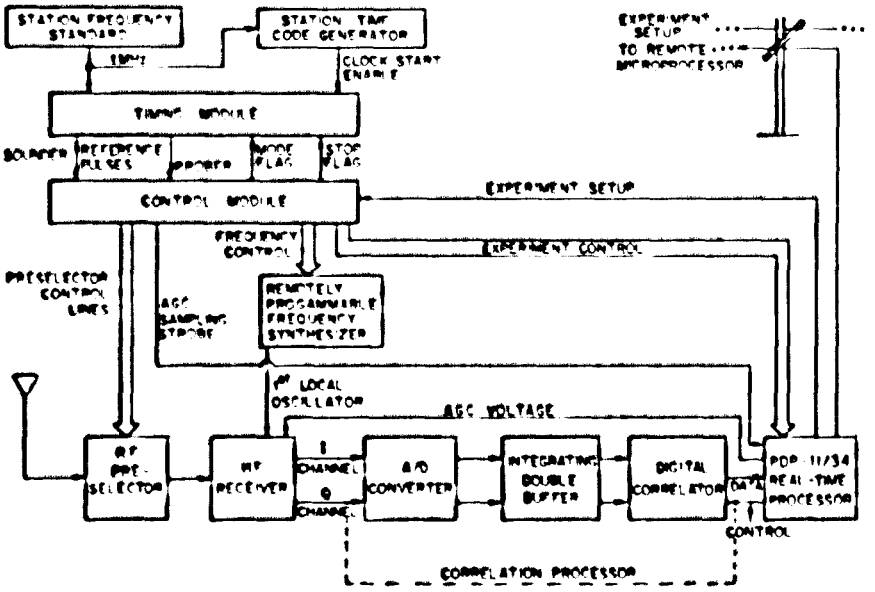

Fig. 28 — Receiving-system block diagram

The receiving equipment consists of five racks of equipment plus a printer-plotter and two computer terminals, as shown in Fig. 29. Two of the racks house the PDP-11/34 and the magnetic tape and disk units. The correlation processor occupies a rack by itself, and the receiver and the timing and control modules occupy the remaining two racks. All of the receiving equipment is contained in a trailer, Fig. 30, for easy transportability. The only receiver-site requirements are access to adequate power and telephones and a sea path for support of the ground wave between transmitter and receiver.

Fig. 29 — Wideband HF Channel Prober receiver/processor

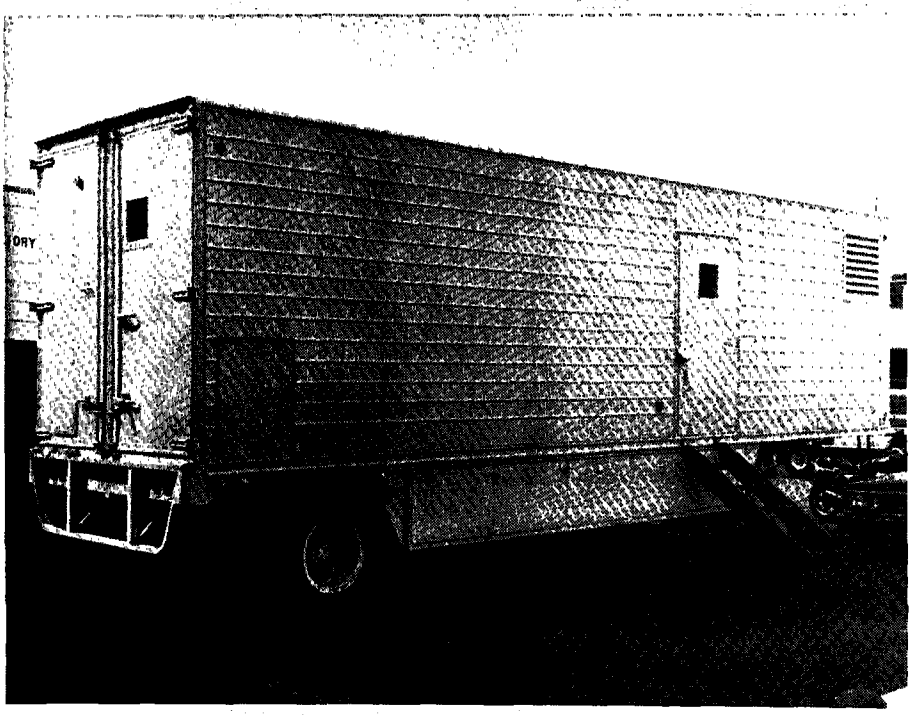

Fig. 30 — Receiving-system trailer

Antenna/Preamplifier

Two different antenna/preamplifier circuits have been designed for the Wideband HF Channel Prober. The first is a short whip transformer-coupled to a Norlin model 304 wideband, high-dynamic-range amplifier, Fig. 31a. Figure 31c contains curves of calculated and measured coupling loss for the whip antenna and its input circuit. These curves show a substantial discrepancy, presumably associated with inaccuracies in modeling the whip antenna. The whip height is 2.5 m, and therefore it should resonate at 30 MHz. The coupling transformer was selected to produce a deliberate mismatch at 30 MHz, causing the system noise, including the effects of receiver back-end noise, to approach quasi-minimum noise [9]. The receiver noise characteristic referred to the whip-antenna input terminals and the curve of quasi-minimum noise (QMN), both expressed as equivalent noise factors, are compared in Fig. 32.

The second antenna/preamplifier consists of a small vertical loop (1-m diameter) coupled to a Norlin model 304 amplifier by a 1:1 turns ratio transformer, as shown in Fig. 31b. Ohmic losses are a significant loss factor for the loop, over and above mismatch losses, because the radiation resistance is less than or comparable to the loop ohmic resistance over the entire HF band. Figure 31c contains a curve of calculated and measured coupling-loss for the small loop antenna and its input circuit. The greater coupling-loss factor of the small loop, compared with the 2.5-m whip, is evident from this set of curves. The measured coupling losses for the loop are seen to provide a good fit to the calculated curve. A 1:1 turns ratio transformer was selected as providing the best system noise factor for the loop over the HF band. System noise factor, including the effects of receiver back-end noise, referred to the loop terminals, is shown in Fig. 32, which illustrates the dominance of receiver noise over QMN external noise in determining system sensitivity with the loop.

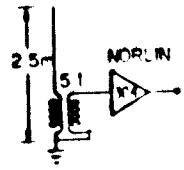

Fig. 31a — Short whip antenna

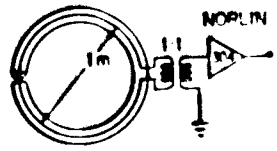

Fig. 31b — Small loop antenna

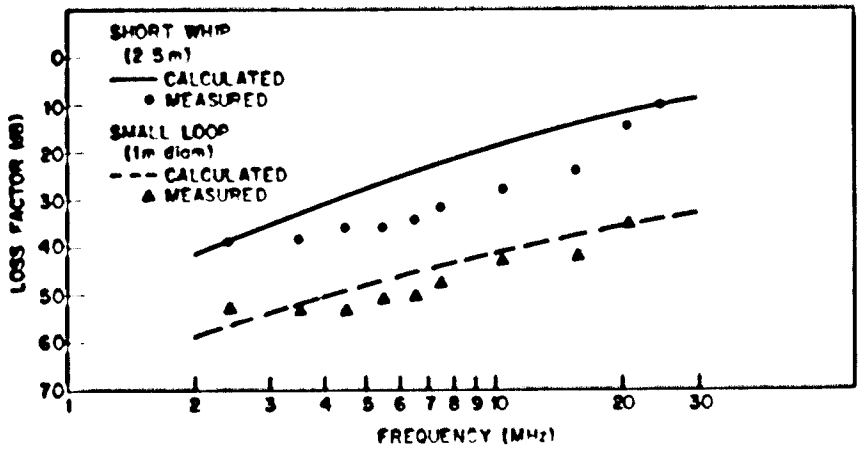

Fig. 31c — Receiving-antenna coupling-loss factor

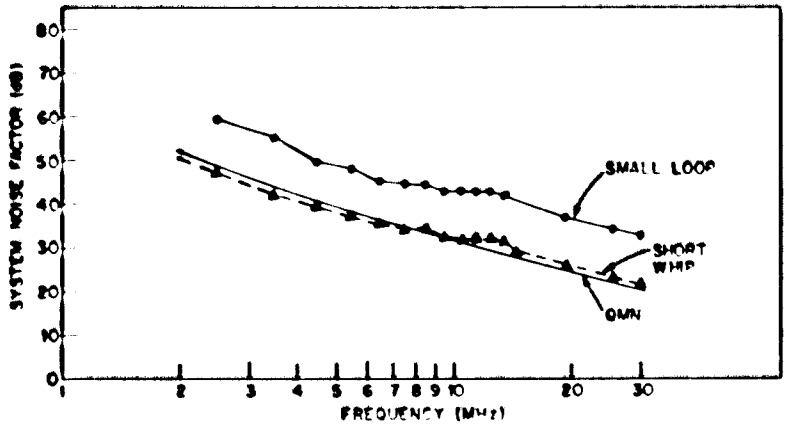

Fig. 32 — System noise factor referred to antenna terminals (QMN is quasi-minimum noise)

The vertical loop was selected as a receiving antenna, despite its poorer noise performance, because of its desirable pattern characteristics. It provides a maximum gain at high elevation angles and a radiation pattern null normal to the plane of the loop. This permits control of the relative amplitude of the ground-wave and sky-wave components by rotation of the loop about its vertical axis. At short ranges, the ground-wave signal tends to be very strong relative to the sky wave, and weak sky-wave returns can be obscured by the time sidelobes of the ground-wave.* Rotation of the loop is used to weaken the ground-wave signal and its time sidelobes, thereby "uncovering" the weak sky-wave returns.

HF Receiver

The HF receiver is a variable-gain, frequency-agile receiver with a bandwidth of either 125 kHz or 1 MHz, depending on the mode of operation. All local-oscillator frequencies are generated from a very stable station standard permitting coherent detection of in-phase and quadrature-phase video outputs. A block diagram of the HF receiver is shown in Fig. 33.

The input attenuator is included for noise-equalization purposes. It provides a means for reducing the dynamic-range requirements of the receiver in the presence of a dominant external noise whose spectral density varies significantly over the HF band. The input attenuator consists of four separate attenuators, each adjustable between 0 and 10 dB in 1-dB steps. Each attenuator is intended to cover a different subrange of the HF band. Attenuator switching is controlled by the control module which, depending on the operating frequency, switches one of the four attenuators into the circuit. The attenuators are coaxial, metallic-film, resistor pi-sections, and they have negligible insertion loss. Switching is accomplished by TTL logic driving reed relays.

The RF preselector restricts the input-frequency spectrum to the HF subband of interest. The preselector consists of sixteen 1-MHz-bandwidth filters covering the range from 1 to 17 MHz, one 3-MHz-bandwidth filter covering the range 17 to 20 MHz, and two 5-MHz-bandwidth filters covering the range 20 to 30 MHz. Filter switching is controlled by the control module according to the frequency. The filters are all of the elliptic-function type with equal ripple in the pass and reject bands. The reject band response is at least −60 dB. The module was part of a Bendix model R-1652 wideband surveillance receiver. A typical 1-MHz-bandpass filter characteristic is shown in Fig. 34. Preselector insertion loss, averaged over the filter passband, is shown in Fig. 35.

The first mixer is a Mini-Circuits Laboratory model ZAD-3B double-balanced mixer. The mixer takes a +7-dBm local-oscillator drive and has a nominal 1-dB compression point of +1 dBm. Insertion loss is approximately 6 dB over the band of interest and isolation between local oscillator and IF ports is of the order of 40 dB.

The first local oscillator is a PTS model 160 direct-frequency synthesizer, which is remotely controlled by the control module so as to heterodyne the input signal to the 39.5-MHz IF. This is the same model used in the exciter down-converter.

The IF filter is a 1-MHz, six-pole, modified Butterworth tubular bandpass filter in the Prober mode and a 125-kHz crystal filter with an approximately Gaussian characteristic in the Sounder mode. Frequency-response characteristics of these filters are given in Figs. 36 and 37. Filter switching is governed by the control module. Insertion loss for the 125-kHz filter is 13 dB. Attenuation has been added in series with the 1-MHz filter to equalize the gain for the two paths.

*The time sidelobes referred to here are those associated with the correlation function of the PN sequence (cf. Fig. 17) rather than those resulting from the nonlinear phase characteristic of the exciter and/or receiver. These sidelobes persist over an interval equal to twice the duration of the PN sequence and therefore fill the entire pulse-response interval.

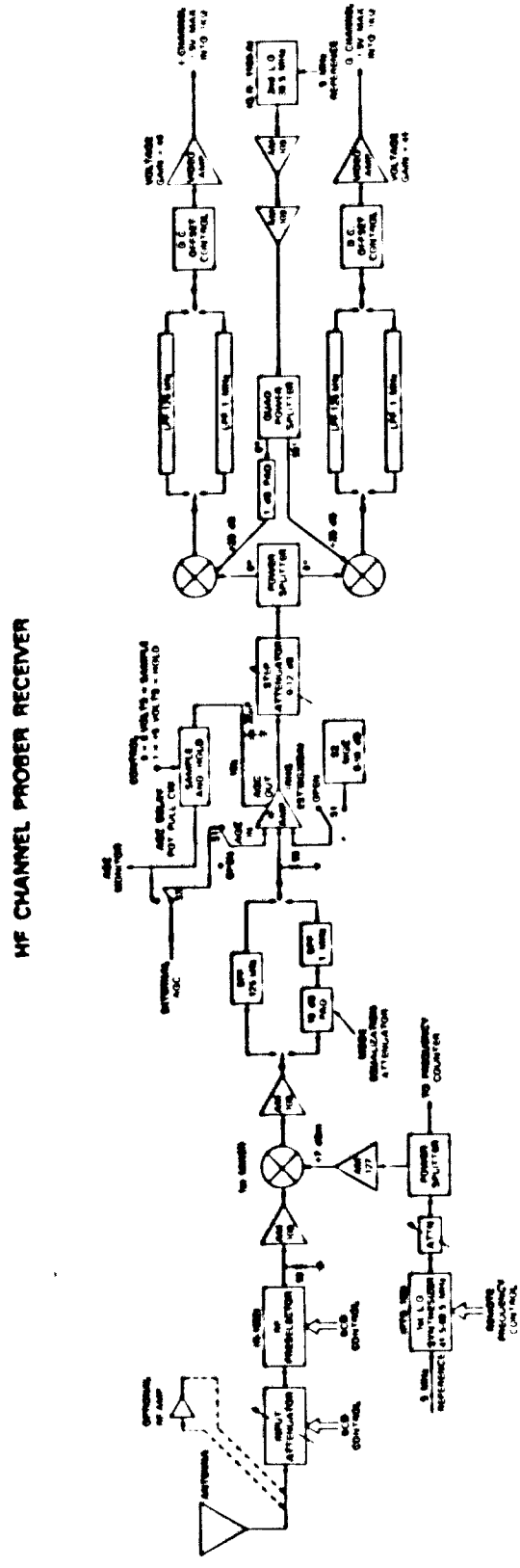

Fig. 33 — HF-receiver block diagram

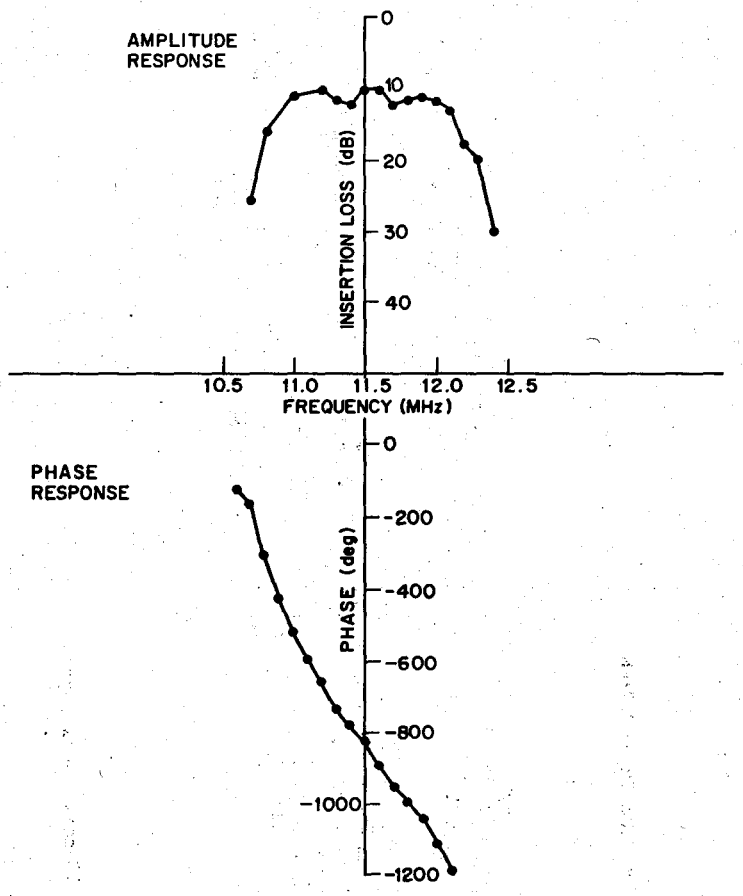

Fig. 34 — Receiver-preselector filter characteristic, 11 to 12 MHz

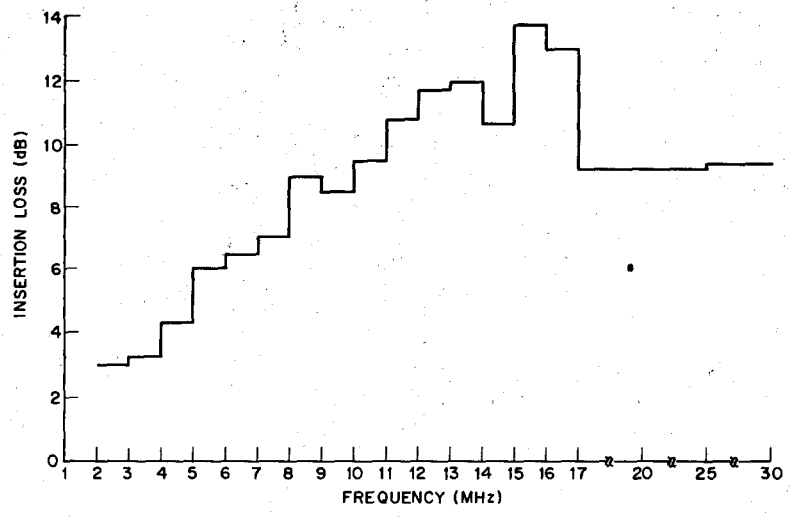

Fig. 35 — Preselector filter insertion loss

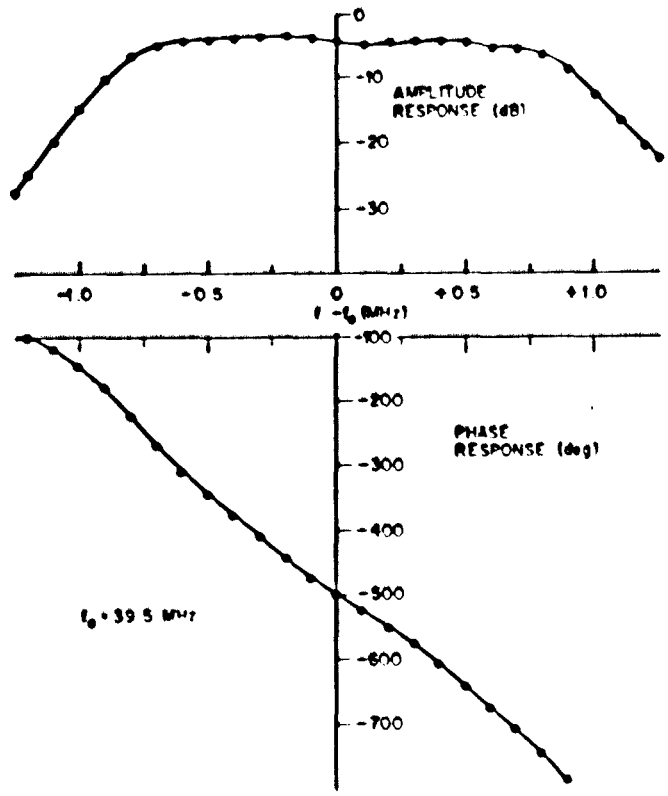

Fig. 36 — Receiver IF-filter response, Prober mode

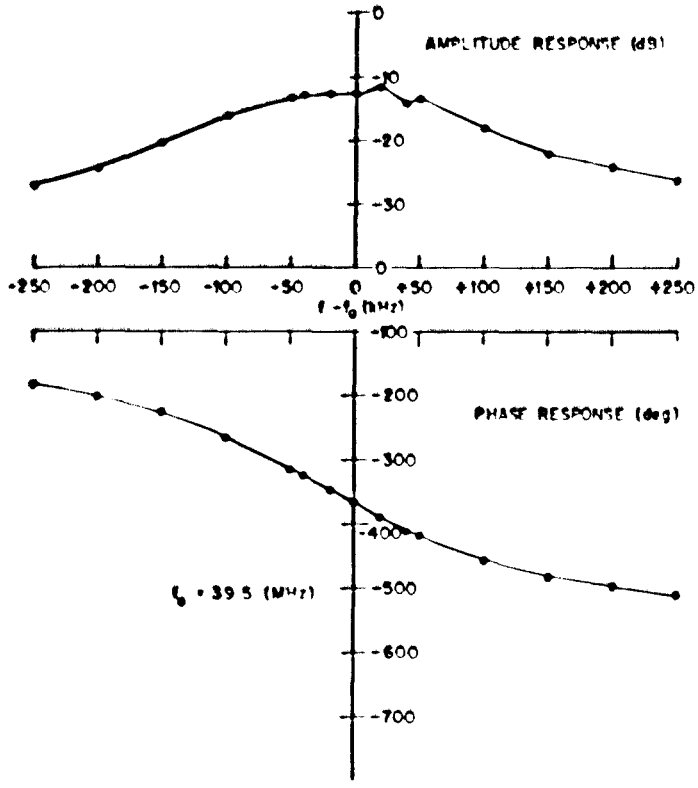

Fig. 37 — Receiver IF-filter response, Sounder mode

The IF amplifier is a customized version of a commercially available amplifier (RHG Electronics Laboratory, Inc., model EST-39G28BA). The amplifier has a maximum gain of 82 dB, a center frequency of 39.5 MHz, a 3-dB bandwidth of 5.6 MHz, a 1-dB compression point of +15 dBm, a noise figure of 2.5 dB, and a measured third-harmonic intermodulation distortion intercept point of +30 dBm.* The amplifier was designed for operation either in a fixed-gain mode or in an AGC mode (switch S1, Fig. 33).

The AGC control characteristic of the amplifier is shown in Fig. 38. The amplifier has been modified so that it can accept an internally generated or an externally generated AGC voltage (switch S3, Fig. 33). When the switch is in the external-AGC position, the AGC voltage is generated in the PDP 11/34 computer.

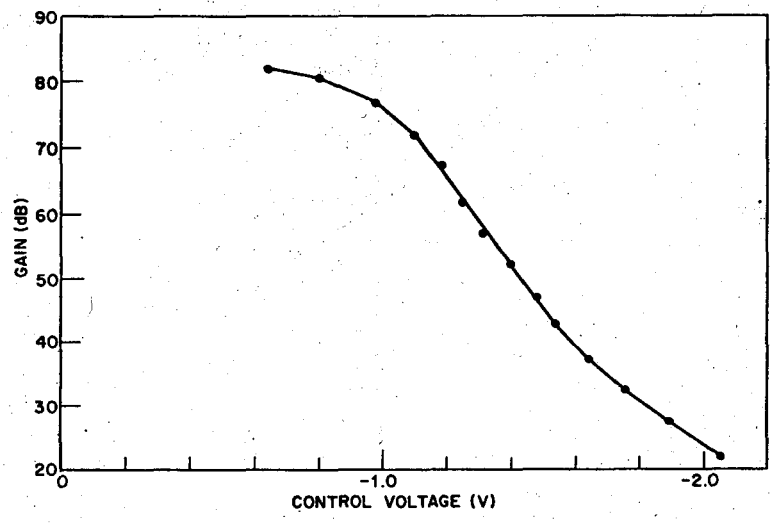

Fig. 38 — IF-amplifier AGC control characteristic

Computer-controlled AGC is the preferred mode of operation. In this mode of operation the gain of the IF amplifier is controlled by a voltage generated in the real-time processor by its sampling of the I and Q voltage outputs from the receiver. This sampling process is done once per correlation during an "idle" sequence of the signal format. The idle sequence is an ordinary PN sequence during which the signals are not used in the correlation calculation. The purpose of the idle sequence is to allow time for all switches and synthesizers to settle, to allow for timing differences, to allow for transit-time delay between transmitter and receiver, and to permit time for establishing an appropriate value of IF-amplifier gain. Once established, the IF-amplifier gain is held constant for the duration of a correlation cycle, which can vary from 90 ms (integration = 1) to 0.5 s (integration = 8). The time period for sampling the receiver output for AGC purposes is defined by the control module. The AGC loop includes the IF amplifier, the video section of the receiver, and an analog-to-digital converter, which is part of the correlation processor but which connects directly to the real-time processor during the idle sequence.

The control algorithm implemented by the computer limits the IF-amplifier output to an average output-power level of −9 dBm. For the quoted intercept point of the amplifier, this implies that third-order intermodulation distortion due to the IF amplifier will be down at least 78 dB relative to the maximum output signal.

*The intermodulation distortion was measured at fixed gain with the output video detector disconnected and with the AGC delay threshold set for maximum delay.

An alternative mode of AGC operation involves the use of an AGC voltage internally generated within the IF-amplifier. The IF amplifier-generated AGC voltage has a threshold controlled by the setting of the AGC delay potentiometer. This controls the bias on the AGC rectifier diode, which controls the signal level at which AGC action commences. This level is set to its highest value (maximum delay) to minimize intermodulation distortion introduced by the AGC rectifier diode. The AGC voltage is sampled, smoothed, and held in a sample-and-hold circuit for the duration of the correlation cycle. This results in a fixed-gain amplifier whose gain is set just prior to the start of correlation according to the signal level prevailing at that time. The AGC sample period is determined by a 2-ms sampling pulse generated in the control module. The sampling pulse is generated during the idle sequence of the correlation cycle and is suitably delayed relative to the time of frequency switching so that all mechanical and electronic components have had time to settle. The sampled signal is averaged over a 1-ms time interval in a low-pass filter integral to the sample-and-hold circuit. Amplifier-controlled AGC, with the AGC threshold delay set to maximum, results in a maximum IF-amplifier output level of +10 dBm. Intermodulation distortion introduced by this level of output signal can be as high as 40 dB below the maximum output signal.

The IF amplifier is followed by an IF attenuator, a power splitter, and a pair of high-dynamic-range quadrature mixers (Mini-Circuits Lab, model ZAY-1B). The mixers require +23 dBm of local-oscillator drive, and they have a nominal 1-dB compression level of +15 dBm, a nominal insertion loss of 6 dB, 40 dB of isolation between LO and RF ports, and 40 dB of isolation between the LO and IF ports. The local-oscillator frequency is 39.5 MHz for beating of the IF signal to baseband. The local-oscillator signal is provided by a General Radio (GR) model-1146A phase-locked-loop synthesizer, operated at fixed frequency, identical to the 39.5-MHz carrier source in the transmitter exciter. Both the PTS-160 and the GR-1146A are phase locked to the 5-MHz station standard, resulting in a phase-stable receiver.

The second mixers (I and Q) are followed by seven-pole, tubular, low-pass filters of Butterworth design and negligible insertion loss. Depending on mode, filters of 125-kHz or 1-MHz bandwidth are switched into the circuit. Response characteristics of these filters are given in Figs. 39 and 40.

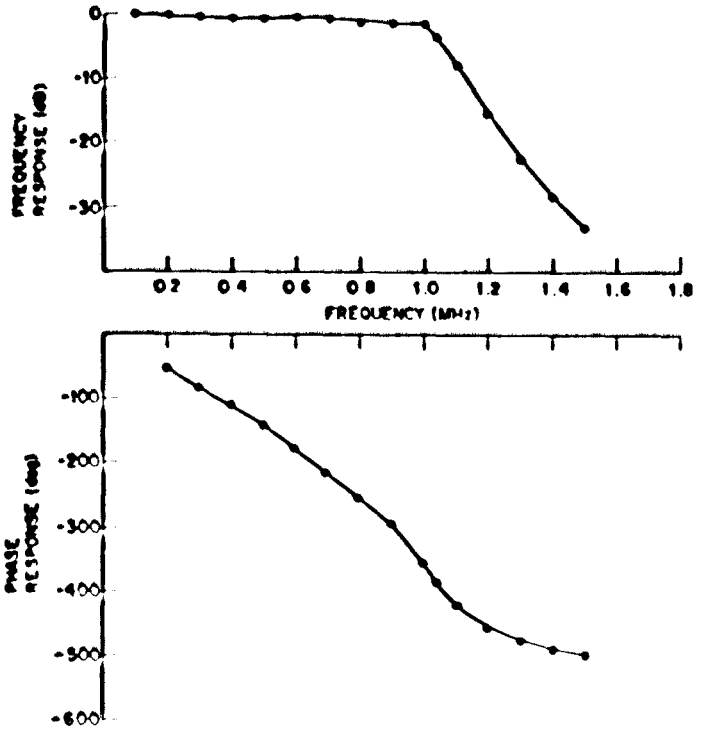

Fig. 39 — Receiver low-pass-filter response, Prober mode

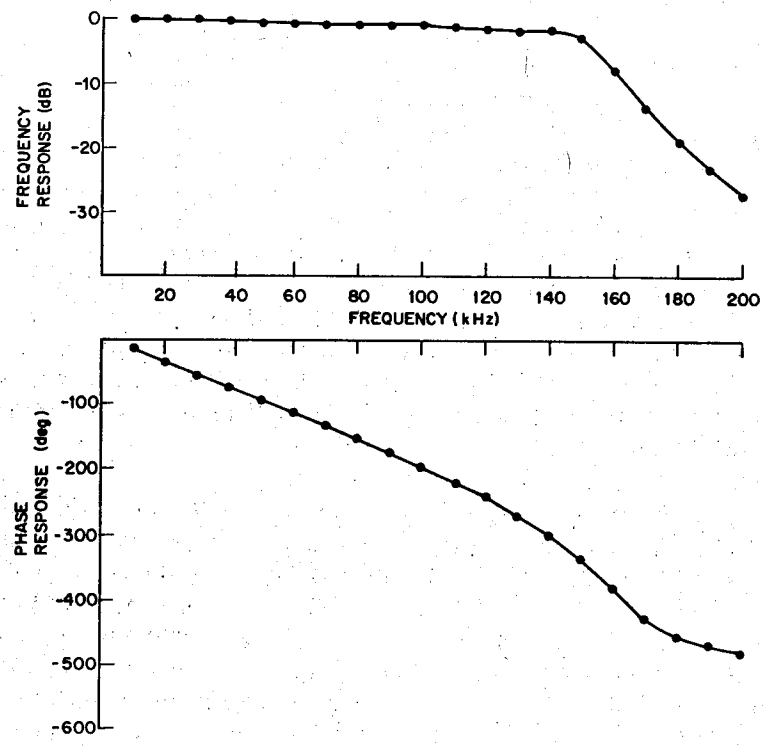

Fig. 40 — Receiver low-pass-filter response, Sounder mode

The video amplifiers are Optical Electronics Inc. model-9412 operational amplifiers with a gain-bandwidth product of 3×10^8, an output voltage swing of ± 10 V into 50 Ω, a slew rate of ± 200 V/μs and an overload recovery time of 300 ns. The amplifiers are configured for a voltage gain of 44 (41 for Q Channel) into a 1000-Ω load (Fig. 41). The power gain, assuming a 50-Ω input impedance, is 20.0 dB.

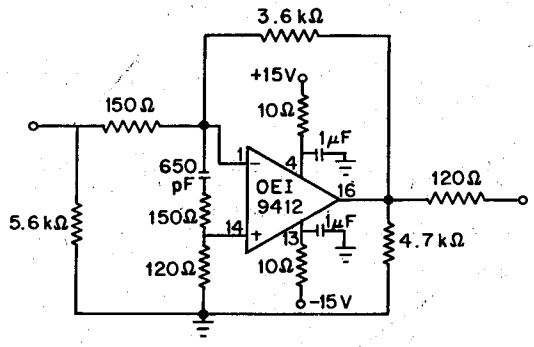

Fig. 41 — Video-amplifier schematic

With IF-amplifier gain limited by AGC action, and assuming computer controlled AGC, the video-amplifier output will be limited to ± 1.77 V (peak) for the signal-dominated case and 0.8 V (rms) for the noise-dominated case. These translate to an average output power of −2 dBm. Taking account of receiver back-end gains and losses, this translates to an IF-amplifier average power output of −9 dBm. In the case of amplifier-controlled AGC, the controlled output level of the IF amplifier is determined by the setting of the AGC delay threshold potentiometer. The output power can be varied

between plus and minus 10 dBm, depending on the potentiometer setting. Given the output of the IF amplifier, the level of input to the correlation processor is then controlled by the IF attenuator, which is adjusted so as to accommodate the received signals without excessive signal clipping.

Because of its intended use as an instrument for defining the wideband pulse response of the HF ELOS channel, the pulse response of the Wideband HF Channel Prober receiver itself is of great interest. Examples of the receiver pulse response are shown in Figs. 42, 43, and 44. Figure 42 shows the receiver sounder-mode pulse response, for an HF frequency of 3.5 MHz, (a) at the output of the IF-amplifier, and (b) at the video-amplifier output. The IF-amplifier output shows negligible degradation of the pulse shape due to enhanced time sidelobes after the pulse passes through the preselector and IF filters. This is readily explained by the fact that the signal bandwidth is small (125 kHz) compared to the preselector filter bandwidth and by the fact that the IF filter is a Gaussian filter. Figure 42b shows evidence of time sidelobes generated in the receiver back end, most likely due to the seven-pole, 125-kHz-bandwidth, low-pass Butterworth filter. The amplitude of these time sidelobes, as estimated from Fig. 42, is −21.5 dB.

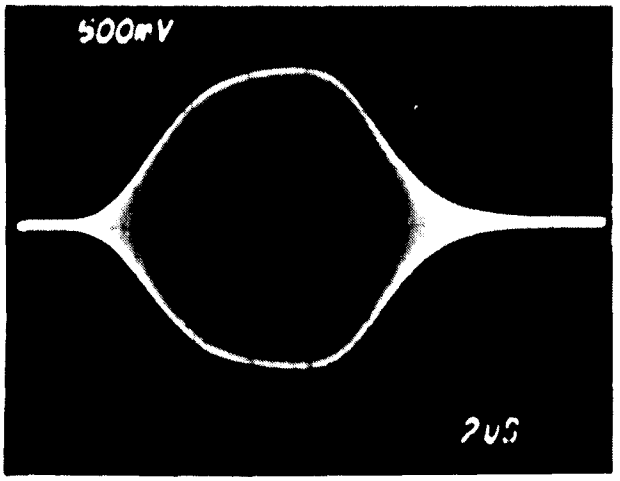

(a)

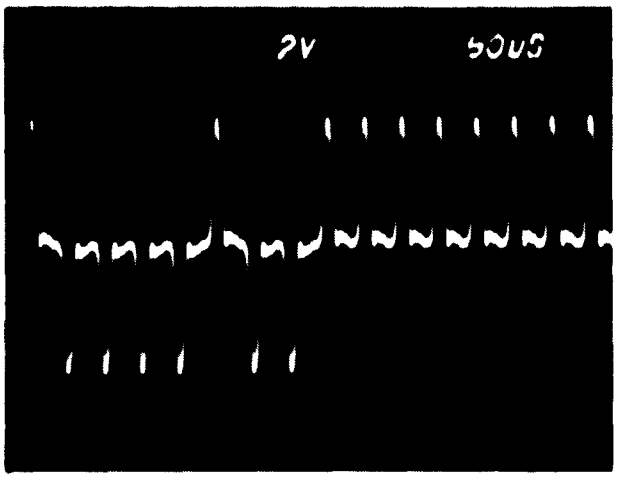

(b)

Fig. 42 — Receiver pulse response. Sounder mode. 3.5 MHz
(a) IF output (b) video output

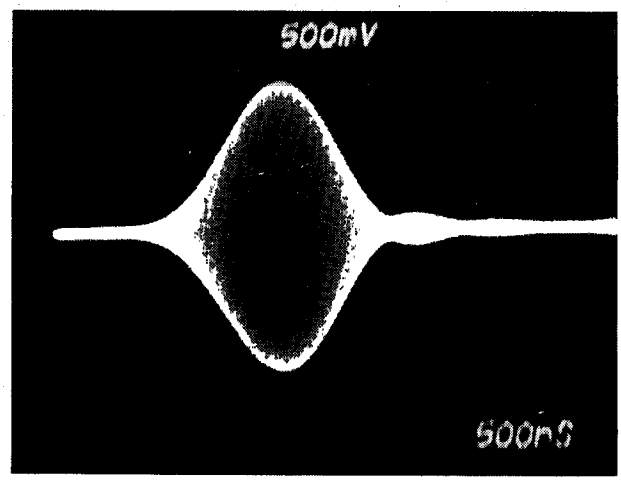

(a)

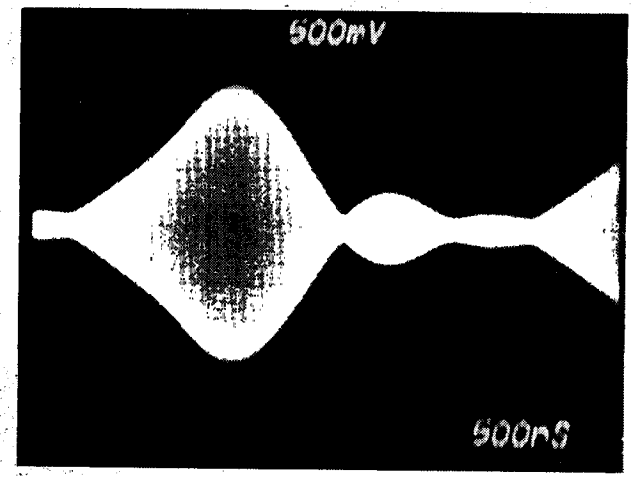

(b)

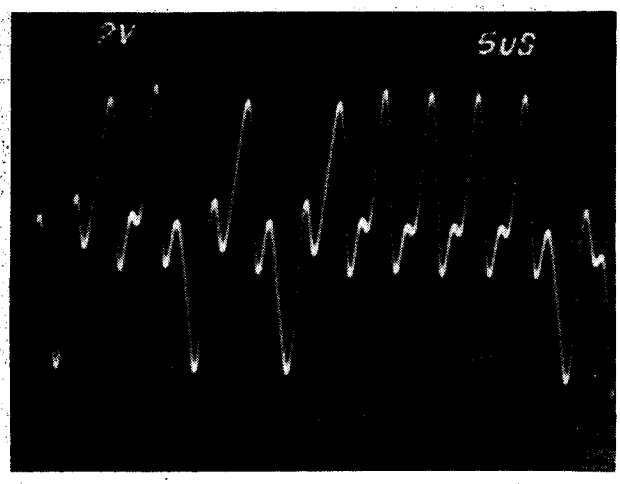

(c)

Fig. 43 — Receiver pulse response, Prober mode, 3.5 MHz: (a) IF output without preselector (b) IF output with preselector (c) video output with preselector

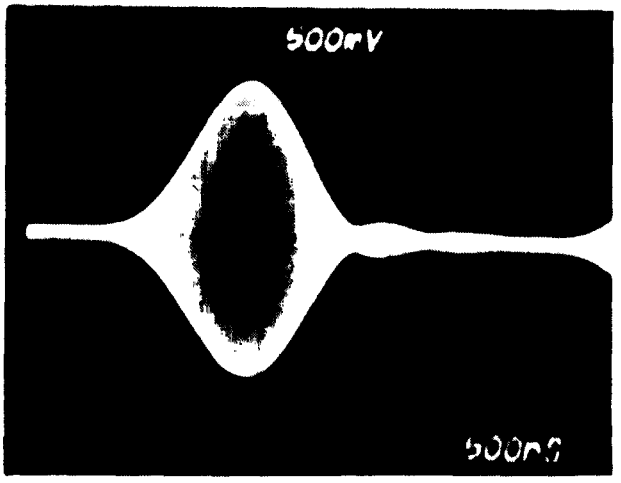

(a)

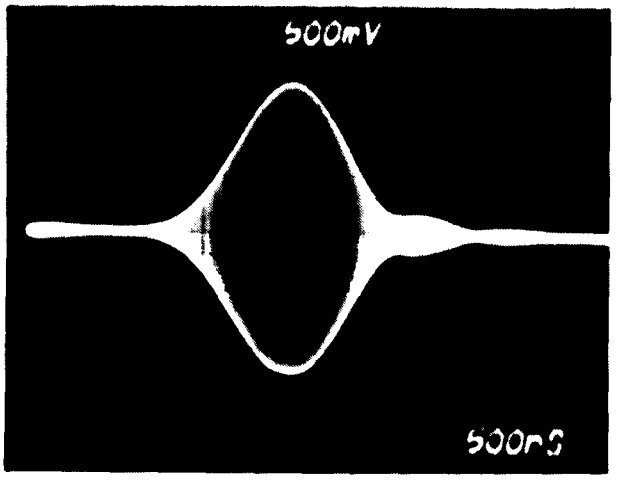

(b)

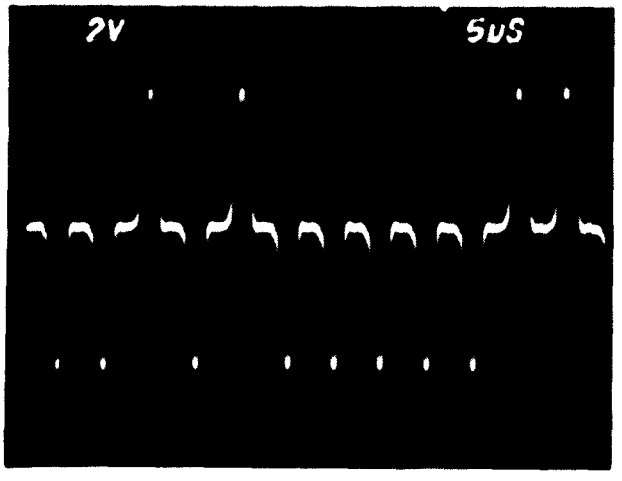

(c)

Fig. 44 — Receiver pulse response, Prober mode, 27.5 MHz: (a) IF output without preselector (b) IF output with preselector (c) video output with preselector

Figure 43 shows the receiver pulse response for the Prober mode at an HF frequency of 3.5 MHz. In this case the signal bandwidth is the same as the preselector bandwidth, and Figs. 43a and 43b present clear evidence for the deleterious effect of the preselector input filter on the time sidelobes. Figure 43c shows the output of the video amplifier. The time sidelobes evident in this curve are of the order of −14.5 dB and are consistent with the sidelobe levels observed at the IF amplifier output.

Figure 44 is the same as Fig. 43 except for the frequency, which in this case is 27.5 MHz. At this frequency the preselector bandwidth is 5 MHz, and consequently the preselector filter has a substantially curtailed effect. Figure 44c shows very low time sidelobes, and these are most likely the result of the seven-pole, 1-MHz-bandwidth, low-pass Butterworth filter. The time sidelobes, in this case, are estimated to be −27.5 dB.

Correlation Processor

The correlation processor consists of four separate modules: the input buffer, the correlator, the computer interface, and the timing and control unit. A block diagram of the correlation processor is shown in Fig. 45.

The input buffer consists of a sample-and-hold module, a 12-bit analog-to-digital (A/D) converter for both the I and Q channels, and an integrating double buffer. The A/D converter sample resolution is 0.5 μs in the Prober mode, and the sampling rate is 250 kHz (4-μs sampling period). During a single frame of the correlation cycle, the pulse response is evaluated at a series of 2047 points spaced by the sampling period. During each subsequent data frame, the sampling window is shifted by 0.5 μs and the pulse response in the adjacent set of points is evaluated. Eight repetitions (frames) result in a delineation of the channel pulse response to a 0.5-μs resolution. A similar procedure applies in the case of the Sounder mode, except that the sample resolution is 4 μs and the sampling rate is 31.25 kHz (32-μs sampling period).

The integrating double buffer uses one half of its memory as an input buffer for storing new data, while the other half acts as an output buffer to the correlator. It represents a convenient place for signal integration, which serves a dual purpose: (1) signal-to-noise ratio improvement and (2) reduction of the system throughput rate. The integrating double buffer is capable of summing the results of one, two, four, or eight contiguous PN sequences.

The correlator consists of 64 separate correlators (32 for I and 32 for Q) operating in parallel. Data from the integrating double buffer are read into the correlators at an 8-MHz rate. Sums or differences of adjacent chips are formed and read into the correlator as warranted by the sequence. This reduces the number of data elements from 2047 to 1023 plus an odd or unpaired term. In the Prober mode, 32 correlations (2047 chips or 1023 pairs) are completed in 128 μs, for an average data rate of 250 kHz on each low-speed output-data bus. Upon completion of a given set of correlations, the process is repeated 64 times for a total of 2047 correlations in an 8-ms period. At each repetition the stored transmitter replica (PN sequence) in the correlator is rotated to match a different set of signal delay times. In the Sounder mode the process needs only to be repeated eight times to completely define a set of 255 correlations per 8-ms PN-sequence interval.

The computer interface is a first-in/first-out (FIFO) stack designed to act as a data spool between the high-speed correlator and the slower real-time processor. The FIFO buffer is actually three 16-bit stacks: one for the I signal value, one for the Q signal value, and one for storing the signal (tap) delay relative to some arbitrary reference. The capacity of the stack was set to accommodate 255 separate I and Q value pairs. This assures no stack overflow in the Sounder mode, provided the stack can be emptied by the computer prior to the next influx of correlation products. In the Sounder mode the minimum time between generation of a new set of 255 I and Q value pairs is 90 ms , which converts to an average of 350 μs available for processing each pair of values.

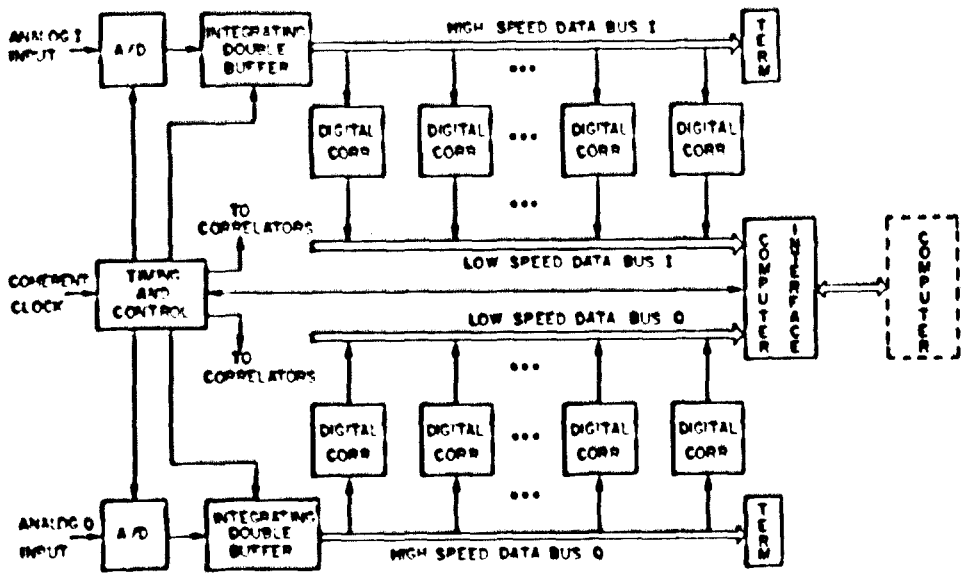

Fig. 45 — Correlation-processor block diagram

In the Prober mode, 2047 correlation pairs are generated during each PN-sequence period. To avoid overflow of the FIFO buffer, some form of data selection must be used. The method implemented is a simple amplitude thresholding where, if either I or Q exceeds a prescribed threshold value, both samples are passed to the FIFO buffer. If both are below the threshold, then the values are discarded. The principle involved in this type of discrimination is that most of the correlator output values are noise and only a few of the total number of outputs correspond to signal. Assuming a sufficiently large value of signal-to-noise ratio (after correlation processing), a simple amplitude-threshold gate should be an effective means of controlling FIFO-buffer overflow.

Because of the variability of signal and noise levels, both in time and in frequency, it is necessary that the threshold be adaptive to the signal environment. The threshold used by the correlator output interface is set by the real-time processor based on the number of samples found in the FIFO buffer during the last PN sequence that was processed. The algorithm is adaptive and is designed to limit the sample pairs to a number smaller than the buffer capacity.

A more complete description of the correlation processor can be found in the final report issued by the manufacturer [10].

Real-Time Processor

The real-time processor is a DEC model PDP 11/34 minicomputer equipped with 128 kwords of RAM memory, 2 kbytes of CACHE memory, an FP11 hardware floating point processor, two 5-Mbyte RL-01 disk units, and a TE-10W magnetic-tape unit. The PDP 11/34 is the primary input device for experiment control parameters. The computer reformats the experiment parameters and manages the communication protocol for transferring the data to the local and remote control modules. The real-time processor controls the operational mode of the correlation processor and accepts and stores data from it. Computer memory is organized as a ping-pong double buffer, with one half acting as the input buffer while the other half is an output buffer to magnetic tape and/or disk for permanent storage. Other operations performed by the real-time processor are "closed-loop AGC" adjustment of IF amplifier gain, adaptive modification of FIFO buffer threshold, and assignment of Prober-mode delay windows. The window gating of received signals in the Prober mode is needed to restrict the quantity of data to limits which the magnetic tape unit can handle in real time.

Software design details of the real-time processor will be given in a separate technical memorandum report.

INITIAL EXPERIMENTAL RESULTS

Initial experimental trials were conducted during February 1982 between the Sea-Echo radar site on San Clemente Island and a receiving station at the Pacific Missile Test Center, Point Mugu, California. A map of the test area is shown in Fig. 46. Transmission tests were initially conducted on 9 February and repeated on 10 February on frequencies of 4.2, 6.3, 13.3, and 26.5 MHz using, at different times, all three of the transmitting antennas and using average power levels ranging between 10 W and 1 kW. Receiver video output signals were monitored at the HF-receiver site. Oscilloscope photos of typical Sounder-mode and Prober-mode video outputs are shown in Fig. 47. The results indicate excellent signal-to-noise ratios for the Sounder mode and satisfactory, although substantially lower, signal-to-noise ratios for the Prober mode. These measurements were made using the 2.5-m whip as a receiving antenna and reflect mainly the power received in the ground-wave mode, the dominant received-signal component. A small sky-wave contribution to the quadrature component of the Sounder-mode signal is evident in Fig. 47a.

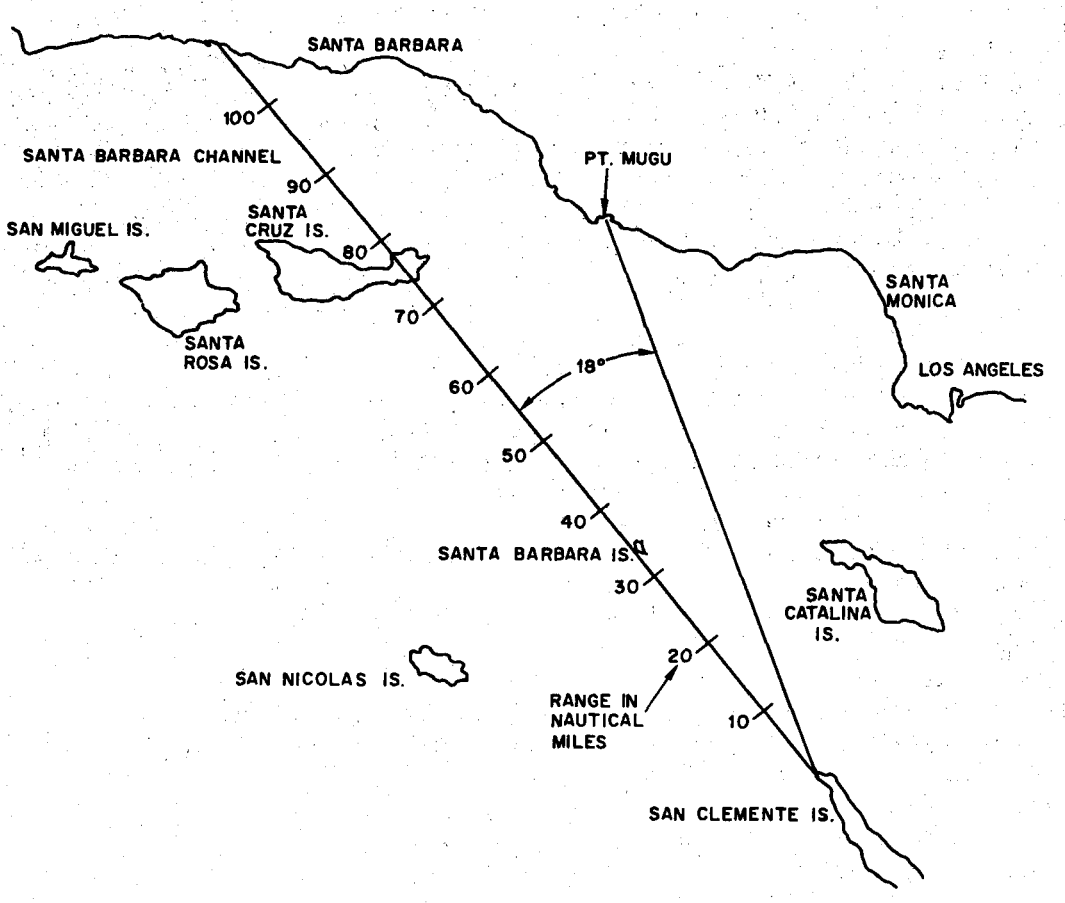

Fig. 46 — Map of test area

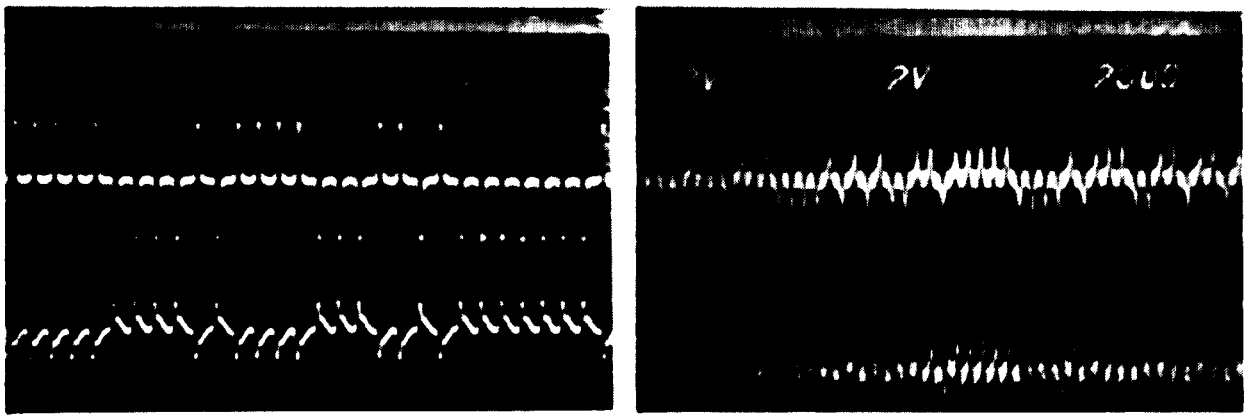

(a) (b)

Fig. 47 — Receiver video recorded at Point Mugu, 6.3 MHz (upper trace, in-phase video; lower trace, quadrature-phase video). (a) Sounder mode (b) Prober mode

Power Measurements

Transmitter power measurements were made with a built-in power monitor which can record incident and reflected power at each antenna of the array. The power monitor was designed for pulses that are longer than those used in the Wideband HF Channel Prober application and, consequently, an alternative, off-line, power-measurement procedure has been devised. This procedure involves the monitoring of the exciter output during operations and, subsequently, repeating the operation with pulses longer than the exciter pulses but of the same amplitude. With this procedure, power measurements as shown in Table 1 were obtained.

Table 1 — Transmitter-Power Measurements

Frequency (MHz)	Av Power (W)		Av Power Corrected (W)	
	Sounder	Prober	Sounder	Prober
2.7	1660	550	1047	78
8.5	4266	1660	2692	240
21.5	1380	380	871	54
28.7	275	71	173	10

Subsequent investigation has revealed that the transmitter power output is sensitive to pulse length and that the actual transmitter power with an 8-μs pulse is approximately 2 dB lower than that measured by the long-pulse substitution method. Similarly, transmitter power for a 1-μs pulse is approximately 8 dB lower than that measured with the long pulse. Table 1 contains additional entries showing transmitter power corrected for the pulse-width dependence. These corrected values show a ratio of Sounder-mode to Prober-mode power of 10 to 12 dB. This ratio was generally confirmed by signal-level measurements at the receiver site.

Sounder-Prober transmitter-power equalization has been accomplished by altering the levels of exciter drive to the power amplifier between the two modes. It has been found that 6 dB more drive in the Prober mode results in roughly equal power. Figure 48 shows output power vs frequency for a single power amplifier operating into a dummy load in both the Sounder and Prober modes.

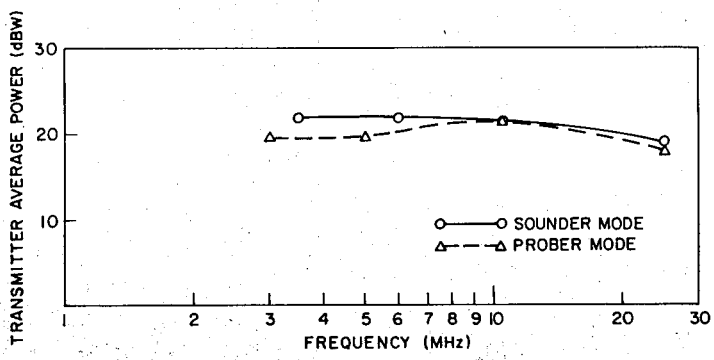

Fig. 48 — Sea-Echo power-amplifier output, operation into dummy load; power amplifier drive levels: (Δ) 12-V (p-p) Prober mode; (O) 7.5 V (p-p) Sounder mode

Sounder-Mode Observations

Sounder-mode (125-kHz bandwidth) observations were originally intended to characterize the ionosphere in a conventional "ionosonde" format. The sensitivity of the instrument, however, results in its providing much more information than is normally available in a conventional ionosonde and in a bandwidth that is not narrow, even considered in the context of modern communication. Examples of sounder observations made with this instrument are shown in Figs. 49 and 50, which are isometric "3-D hidden-line" plots of a series of pulse-response characteristics made on frequencies covering a portion of the HF band. Only frequencies below 10.5 MHz are shown on the ionograms because of picture size limitations of the CRT used for plotting purposes. The presentation is of data uncorrected for AGC gain variations, as is customary in ionosonde displays. The data are, furthermore, thresholded in order to eliminate time sidelobes of the ground wave, which would otherwise clutter the display. The ionosonde format provides the frequency-delay characteristic necessary for the classification of the signal modes. Ground-wave, one-hop E, one-hop sporadic E, one-hop F2, and two-hop F2 modes are evident in Figs. 49 and 50. Ordinary *(O)* and extraordinary *(X)* components of the sky-wave returns are distinguishable and are indicated on the figures.

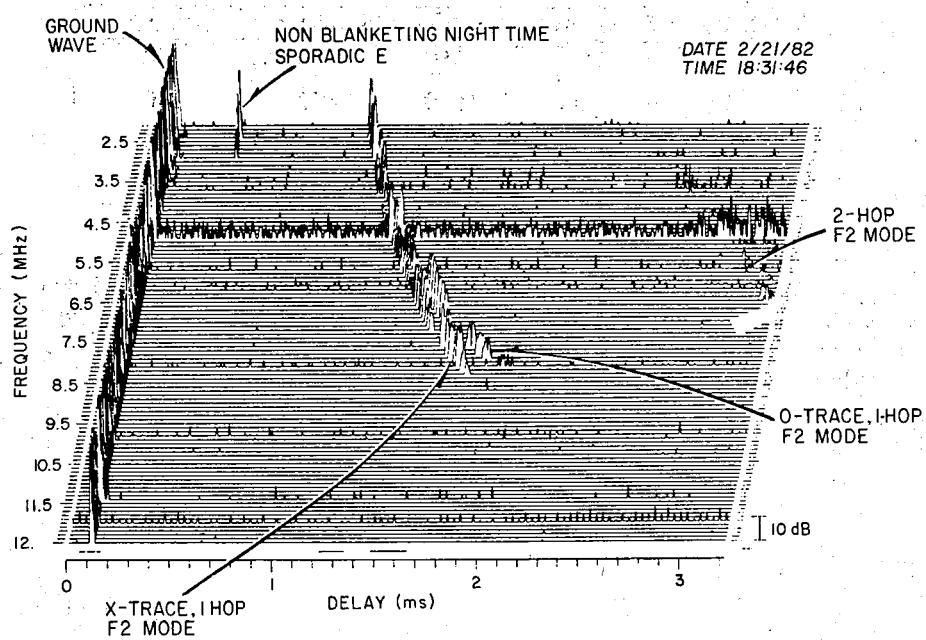

Fig. 49 — Wideband HF Channel Prober ionogram, evening

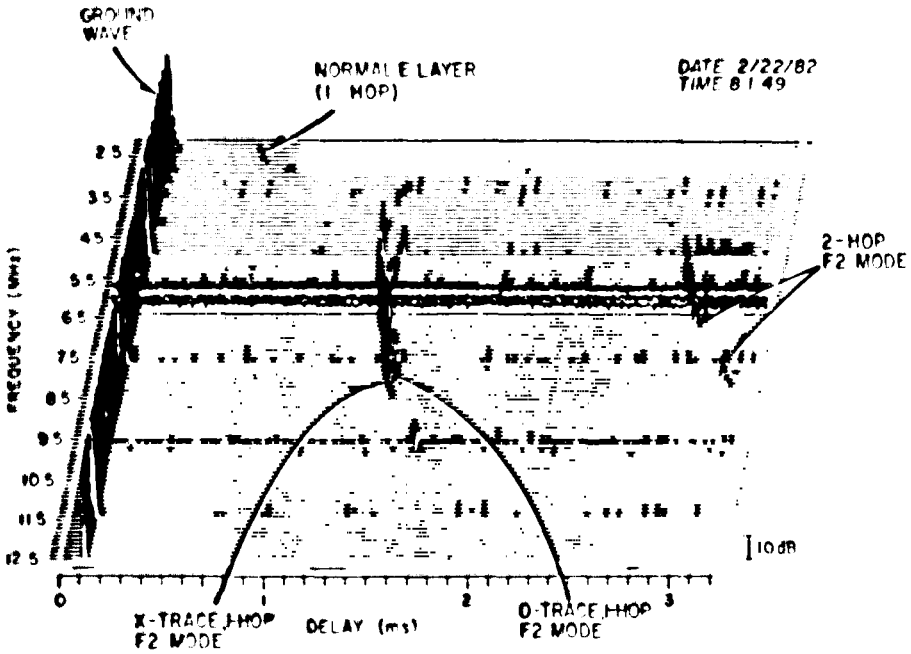

Fig. 50 — Wideband HF Channel Prober ionogram, morning

It is instructive to view the Sounder-mode pulse response at a single frequency. This is equivalent to viewing a single trace of the ionograms of Figs. 49 and 50, with the one difference that the thresholding is dispensed with. An example of such a pulse response is shown in Fig. 51 for a transmitter frequency of 10.4 MHz. It can be readily seen from this figure that the signal-to-noise ratios for the ground wave and one-hop F2 sky wave are 75 and 30 dB, respectively. It is immediately apparent that a substantial body of low-level sky-wave return is obscured by the time sidelobes of the ground-wave signal, which is far and away the strongest signal present. This suggests that the degree of detail available regarding sky-wave modes can be increased substantially by selectively reducing the ground-wave return relative to the sky wave. This can be readily accomplished by taking advantage of the antenna pattern for a vertical loop antenna.

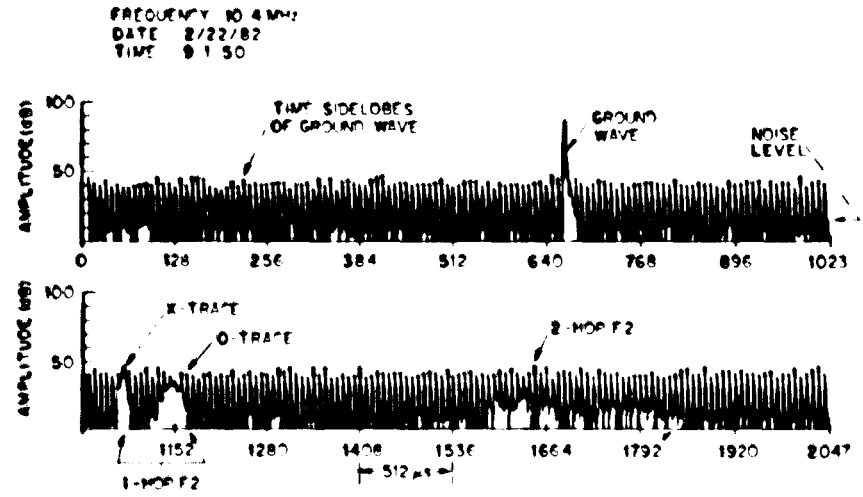

Fig. 51 — Pulse response, Sounder mode, 10.4 MHz

Another interesting aspect of the Sounder data is the presence of nighttime sporadic-E returns. An expanded examination of the sporadic-E pulse reponse, Fig. 52, reveals substantial pulse spreading, evident even with a bandwidth of 125 kHz. Other data indicate a rather complex dependence on frequency. This can most likely be explained in terms of the multilayered nature of nighttime sporadic E. Wideband observations of nighttime sporadic E should reveal details of this structure.

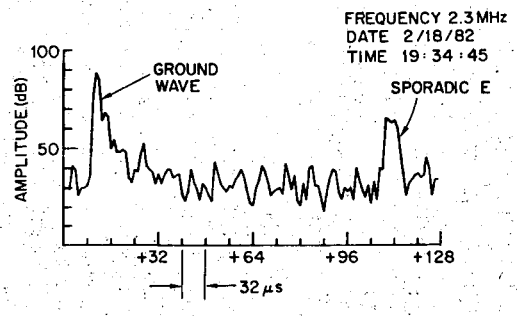

Fig. 52 — Pulse response, Sounder mode, 2.3 MHz

Prober-Mode Observations

In the Prober mode, the number of data samples required to define completely the channel pulse response over an 8-ms interval is much too large to be handled by the signal processor in real time. As a consequence, signal-observation windows, based on Sounder data, are established to limit the volume of data that needs to be processed. In addition, to prevent overflow of the computer interface between the correlator and the computer, amplitude thresholding is used to limit the data that enter the buffer. Prober data are thus confined to preassigned windows, and the data must exceed an adaptively established threshold to be stored.

In viewing the data, one usually selects a window corresponding to a particular signal mode (e.g., the ground-wave, the single-hop F2 layer mode, etc.) and examines that separately. Figure 53 shows examples of the ground-wave signal at frequencies of 5.5 and 8.5 MHz received at the Point Mugu receiving site. Comparison with the system pulse response, as measured during bench tests, indicates negligible pulse dispersion associated with the propagation path at a frequency of 8.5 MHz. This result is observed at all frequencies greater than 8.5 MHz as well. At 5.5 MHz, significant pulse spread is observed, and this seems to be characteristic of the lower HF frequencies. Sea states were generally light during the observation period. Dispersion due to the transmitter power amplifier or antenna cannot yet be ruled out. Further examination using a variety of transmitter configurations is required.

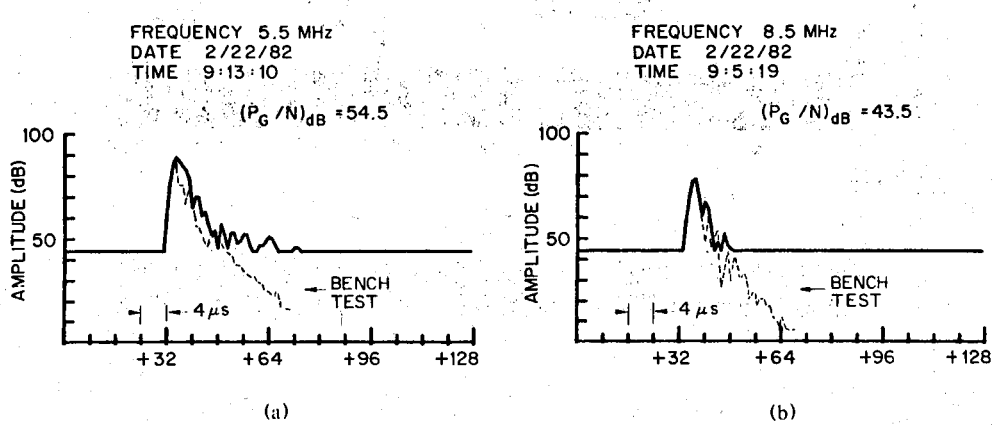

Fig. 53 — Ground-wave pulse response, Prober mode, (a) 5.5 MHz, (b) 8.5 MHz

Observations confined to the one-hop F2-layer time window are shown in Figs. 54 and 55. These are isometric "3-D hidden-line" plots showing signal amplitude in decibels vs signal delay for a series of time cuts and at a fixed frequency. The threshold or "floor" of the curve is established by the actual data threshold of the earliest cut. The data for frequencies of 5.5 MHz and 6.5 MHz indicate the effect of what appears to be a traveling ionospheric disturbance (TID) on the pulse delay and pulse spread of the *O* and *X* components of the one-hop F2-layer mode. Another interesting aspect of Fig. 54 is the presence of a bifurcated *O* return also probably related to the presence of the TID.

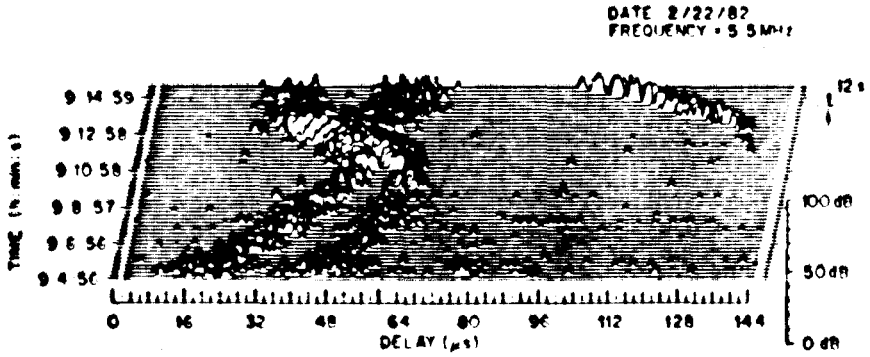

Fig. 54 — Pulse-response time history, Prober mode, one-hop F2, 5.5 MHz

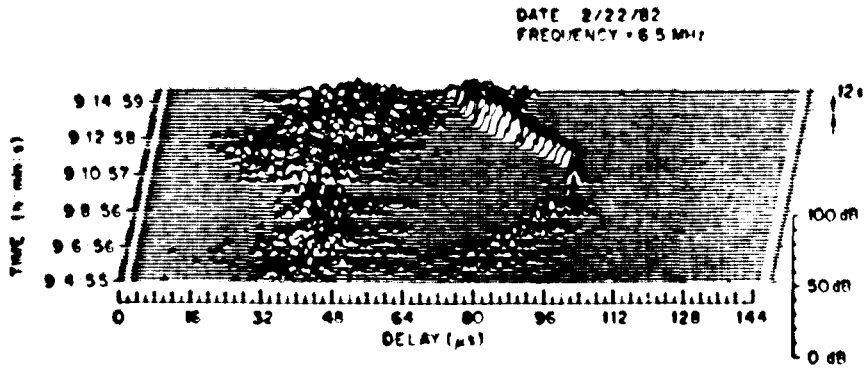

Fig. 55 — Pulse-response time history, Prober mode, one-hop F2, 6.5 MHz

DISCUSSION

Initial measurements with the Wideband HF Channel Prober have demonstrated that the instrument is capable of making wideband measurements of the HF ELOS channel in real time and with the sensitivity and precision anticipated. Acceptable received-signal levels have been obtained in Sounder mode (narrowband) with transmitter average power ranging between 200 and 3000 W. Useful Prober-mode (wideband) data have been obtained with transmitter average power ranging between 10 and 300 W. Preliminary results support the claim that the instrument can be used for defining the channel characteristics of the sporadic-E and the one-hop F2 modes. It is apparent from some of the observations that, under certain special conditions, the one-hop F2 mode can support 1-MHz-bandwidth signals for limited time intervals (cf. Fig. 55). The variability of the delay of the one-hop F2-layer mode propagating through a gravity-wave-modified ionosphere is clearly illustrated in Figs. 54 and 55, and this should be of considerable interest to communication and HF direction finding system designers.

SUMMARY

A coded-pulse radio sounder having a time resolution of 1 μs has been built and tested. The sounder operates in one of two modes, a narrow-bandwidth (125-kHz) Sounder mode and a wide-bandwidth (1-MHz) Prober mode. A correlation receiver reconstructs the channel pulse response characteristic in real time, and the data are recorded on magnetic tape for later processing off-line. The measurement format consists of a narrowband scan through the HF channel, followed by an extensive interval of wideband measurements, followed by a repetition of the narrowband scan. Narrowband operation is used for providing a conventional description of the channel (ionogram for the skywave modes) and also to permit the placement of mode delay acceptance windows to be used with the wide-band mode. Wideband measurements are made continuously for a total period of approximately 15 min, which is deemed, a priori, to be the time for statistical stationarity of the channel.

The Wideband HF Channel Prober is designed to be used with available high-power, wideband HF transmitter and antenna systems and is intended as a probing device for investigating the wideband characteristics of the HF ELOS radio communication channel. Initial measurements have been made over a 126-km overwater path between San Clemente Island, off the coast of southern California, and Point Mugu on the southern-California coast. Results show a great variety of responses for the sky-wave modes, depending on time of day and season of the year and upon the degree of disturbance of the medium. Results showing the variation of dispersion and delay of the one-hop F2-layer modes in response to an apparent TID are illustrated in some of the figures.

ACKNOWLEDGMENTS

The authors thank Dr. J. R. Davis of NRL for originally suggesting this program and for his continuing support throughout. We acknowledge the early contributions of Dr. P. A. Bello, Dr. L. Pickering, and Mr. George Peo, of CNR Inc., and Mr. R. Bauman, of NRL, to the program and especially the contributions of Dr. Bello and Mr. Peo to the development of the hardware processor. We are indebted to Messrs. E. E. Barr and W. D. Myers, of NRL, who were instrumental in the development of the HF receiver and its antenna system. We also acknowledge the contributions of Dr. R. W. Bogle, of Worth Research Associates, for his fine job of preparing the Sea-Echo radar transmitter for operation and for his logistical support during our California operations. Finally, we thank Mr. C. Elliot, of the Program Management Office (Code 0140) of the Pacific Missile Test Center, for his invaluable support during our operations at Point Mugu.

REFERENCES

1. J.L. Wheeler, "Channel Characteristic Measurements of Upper-MF and Lower-HF Surface Wave Propagation over Sea Water," ITT-EPL Project Report 250, ITT Electro Physics Laboratories, Inc., Columbia, Md., Contract N00014-72-C-0441, Feb. 1974.

2. D.E. Barrick, "Theory of HF and VHF Propagation Across the Rough Sea, 2, Applications to HF and VHF Propagation Above the Sea," *Radio Sci.* **6**, 527 (May 1971).

3. P. Hansen, "Measurements of Basic Transmission Loss for HF Ground Wave Propagation Over Seawater," *Radio Sci.* **12**, 397 (May-June 1977).

4. E.C. Hayden, "Delineation of Constraints Imposed by Propagation Factors at HF on Jamming of Ships Communications," Final Technical Report, Project 16-4312, Southwest Research Inc., San Antonio, Tex., Contract N00039-75-C-0481, Dec. 1979.

5. P.A. Bello, L.W. Pickering, G.E. Peo, and K.P. Jauniskis, "Wideband HF Channel Measurement Studies," Project 47, CNR Inc., Needham, Mass., Contract N00173-77-C-0249, Mar. 1979.

6. L.S. Wagner and J.A. Goldstein, "Wideband HF Channel Prober—Timing and Control Modules," NRL Memorandum Report 4933, Aug 1982.

7. M.T. Ma and L.H. Tveten, "A Broadband Antenna Array for Sea Scatter Measurements," OT Report 75-60, Office of Telecommunications, Boulder, Colo., Apr. 1975.

8. D.H. Layton, "A High-Frequency Broadband Transmitter for Monostatic Systems," NTIA-TM-81-59, National Telecommunications and Information Administration, Boulder, Colo., July 1981.

9. W.E. Gustafson and W.M. Chase, "Shipboard HF Receiving Antenna System: Design Criteria," NELC Technical Report 1712, Naval Electronics Laboratory Center, San Diego, Calif., June 1970.

10. G.E. Peo and P.A. Bello, "Wideband HF Channel Analyzer," Project 58, CNR Inc., Needham, Mass., Contract N00173-79-C-0090, Jan 1981.